Dominant role of charged meteoric smoke particles in the polar mesospheric clouds

Liang Zhang[1], Zhongfang Liu[1], Brian Tinsley[2]

[1]State Key Laboratory of Marine Geology, Tongji University, Shanghai, 200092, China
[2]Physics Department, University of Texas at Dallas, Richardson, Texas, 75080, USA

Correspondence to: Liang Zhang (Liangzhang420@tongji.edu.cn)

Abstract. Polar mesospheric clouds (PMCs), composed of ice particles, are sensitive to solar activity and atmospheric dynamics, and have been suggested as a potential indicator of climate change. However, the microphysical processes of PMCs, especially the mechanism of ice nucleation, remain poorly understood. This study presents an analysis of satellite PMC data, which reveals that the mean ice particle radius (r) and concentration (N) in PMCs are primarily influenced by the PMC height (h), rather than by the mean environment temperature (T). Additionally, the ice particle column concentration (N_c) exhibits a surprising decrease with latitude. These results support the hypothesis that charged meteoric smoke particles (MSPs) act as ice nuclei, based on which we propose the charged-MSPs nucleation (CMN) scheme for the PMC formation. In contrast to the conventional growth-sedimentation (GS) scheme, in the CMN scheme the nucleation occurs throughout the PMC altitude range, ice particles grow mainly in situ, and the ice particle radius is determined by the competition for the limited water vapor rather than by sedimentation. The CMN scheme provides new pathways for solar activity and atmospheric dynamics to affect PMCs, and can explain a number of puzzling phenomena in the GS scheme.

1 Introduction

1.1 PMCs

Polar mesospheric clouds are the highest clouds in the Earth's atmosphere, usually forming in the polar mesopause when the temperature drops below 150 K in summer (Rapp and Thomas, 2006), and occasionally occurring in the mid-latitudes (Hervig *et al.*, 2016b; Miao *et al.*, 2022). Polar mesospheric clouds, together with polar mesospheric summer echoes (PMSEs) (Rapp and Lübken, 2004), both associated with ice particles, provide unique physical and dynamical information for the summer polar mesosphere. These ice particles are sensitive to perturbations in temperature and water vapor (Rong *et al.*, 2012), making PMCs susceptible to atmospheric dynamics, including gravity waves (GWs) (Chandran *et al.*, 2012; Gao *et al.*, 2018; Rusch *et al.*, 2017), planetary waves (France *et al.*, 2018; Liu *et al.*, 2015), tides (Fiedler and Baumgarten, 2018; Liu *et al.*, 2016), and inter-hemispheric coupling (IHC) (Gumbel and Karlsson, 2011; Karlsson *et al.*, 2009). The water vapor

released by rocket exhaust has been observed to enhance PMCs (Collins *et al.*, 2021; Stevens *et al.*, 2003), although the
30 long-term effects of space traffic on PMCs remains uncertain (DeLand and Thomas, 2019; Siskind *et al.*, 2013).

Solar ultraviolet (UV) radiation can heat the air and photolyze water molecules (Beig *et al.*, 2008; Shapiro *et al.*, 2012),
so it is straightforward to expect PMCs to be negatively correlated with the solar cycle. However, the 27-day solar cycle in
PMCs is typically ambiguous, unless the superposed epoch analysis method is applied to remove background noise, and the
lag time is only about 0-3 days (Dalin *et al.*, 2018; Robert *et al.*, 2010; Thurairajah *et al.*, 2017), shorter than the at least five
35 days required for the photodissociation (Shapiro *et al.*, 2012). The 11-year solar cycle in PMCs is evident prior to 2002, but
has disappeared over the past two decades, for reasons that remain unknown (Hervig *et al.*, 2019; Vellalassery *et al.*, 2023).
Global warming favors the formation of PMCs in two ways: increased carbon dioxide tends to cool the upper mesosphere
via the terrestrial radiation budget, and increased methane tends to increase the water vapor via oxidation (Lübken *et al.*,
2018). Nevertheless, the corresponding long-term trend in response to global warming has not been confirmed by
40 observations (Hervig *et al.*, 2016a; Kirkwood *et al.*, 2008), and whether the PMC can serve as an indicator of climate change
has been a topic of intense debate.

1.2 Nucleation processes in PMCs

The ice nucleation process contributes the most significant uncertainties to the microphysical process of PMCs.
Homogeneous nucleation is unlikely to occur at typical mesospheric supersaturation levels (Tanaka *et al.*, 2022), and
45 heterogeneous nucleation is thought to be responsible for the formation of ice particles by providing pre-existing ice nuclei,
for which the MSPs have been proposed as the most likely candidate (Duft *et al.*, 2019; Hervig *et al.*, 2012). Meteoric smoke
particles are produced by meteor ablation and recondensation and are abundant in the upper mesosphere, with radii ranging
from sub-nanometre to nanometre sizes (Plane, 2012; Scales and Mahmoudian, 2016).

The charged-MSPs have also been proposed as candidates for ice nuclei, given that the charges on MSPs can effectively
50 reduce the critical radius (r_c) at low temperatures (Gumbel and Megner, 2009; Megner and Gumbel, 2009). However, the
variability, distribution and charging process of MSPs remain unclear (Antonsen *et al.*, 2017; Dawkins *et al.*, 2023; Hervig *et al.*, 2022; Knappmiller *et al.*, 2011; Li *et al.*, 2022), and this proposal has not yet gained widespread support (Duft *et al.*,
2019; Plane *et al.*, 2023). The mobility of electrons is much greater than that of positive ions, so MSPs in the upper
mesosphere tend to collect electrons, with rocket-borne measurements showing that about 10% of MSPs are negatively
55 charged (Plane *et al.*, 2014; Robertson *et al.*, 2014). It should be noted that the galactic cosmic rays can ionize the
troposphere and produce charged molecular clusters that grow much faster than neutral clusters, and the so-called ion-
mediated nucleation has long been proposed as an important way for the formation of cloud condensation nuclei in the
troposphere (Yu *et al.*, 2018; Yu and Turco, 2000).

The PMCs are located in the D-region of the ionosphere, where solar winds can exert an influence. The electric potential
60 of the ionosphere relative to the Earth's surface is about 250 kV, maintained by the global thunderstorms and electrified
clouds (Williams and Mareev, 2014). The dawn-dusk component of the interplanetary magnetic field (*IMF B_y*) can modulate

the polar ionospheric electric potential through the Lorentz electric field, $E_z = B_y \times V_x$, where the V_x is the solar wind velocity. As the *IMF B_y* increases, the electric potential in the Southern Hemisphere (SH) polar region increases by ~20 kV on average, thereby decreasing the electron density and the concentration of negatively charged-MSPs. In contrast, the response in the Northern Hemisphere (NH) is opposite (Lam and Tinsley, 2016; Tinsley and Heelis, 1993). Zhang *et al.* (2022) have demonstrated a positive/negative correlation between the *IMF B_y* and the ice particle radius of PMCs in the SH/NH with a lag time of about zero days, providing evidence in favor of the charged-MSPs acting as ice nuclei.

1.3 The "growth-sedimentation" scheme for PMC formation

The growth-sedimentation process is currently the most commonly used scheme to describe the formation of PMCs. In the GS scheme, ice nucleation occurs primarily at the top of the PMC, and then ice particles grow by water vapor deposition and fall downward under gravity, until they sediment out of the supersaturated zone and sublime (Hultgren and Gumbel, 2014; Rapp and Thomas, 2006). The lifetime of ice particles is also influenced by upward winds and diffusion. In the GS scenario, ice particle concentrations are higher at the top of the PMC and ice particle radii are larger at the bottom of the PMC due to ice particle growth and sedimentation, as supported by observations (Hervig et al., 2009a; Hultgren and Gumbel, 2014).

However, the conventional growth-sedimentation scheme for PMC formation faces a number of challenges. First of all, it seems unreasonable that ice nucleation takes place primarily at the top of the PMC, since the saturation levels throughout the PMC altitude range all favor PMC formation. Observed data indicates that the PMC is approximately in equilibrium with the surrounding environment, which is inconsistent with the dominant role of the sedimentation in the GS scheme (Christensen et al., 2016; Hervig et al., 2009c).

In the GS process, MSPs larger than the critical radius ($r_c \approx 1$ nm) are assumed to act as ice nuclei (Hervig *et al.*, 2012; Rapp and Thomas, 2006). However, the simulations involving mesospheric circulations showed that the large MSPs ($r > r_c$) are transported upwards along with the strong updrafts in the summer mesosphere, then transported into the winter mesosphere by the meridional winds, and finally sink to the stratosphere by downwelling (Megner et al., 2008a; Megner et al., 2008b). The global mass redistribution of MSPs results in a pronounced reduction of MSP concentration and lifetime in the summer mesosphere, thus there are not enough large MSPs in the summer polar mesosphere to act as ice nuclei.

In the GS process, the concentration of ice particle should decrease continuously from the top to the bottom of the PMC, but observations reveal the multi-layered structure of ice particles (Gao *et al.*, 2017; Kaifler *et al.*, 2013; Schäfer *et al.*, 2020). Moreover, the PMCs enhanced by the rocket exhaust plumes exhibit an inverse altitude dependence, with larger ice particles observed at higher altitudes (Stevens *et al.*, 2012). In the GS process, the entire life cycle of ice particles in PMC includes nucleation, growth, sedimentation and sublimation, which can take up to tens of hours (Rusch *et al.*, 2017; Wilms *et al.*, 2016), whereas PMCs vary more rapidly in observations (Megner *et al.*, 2018; Rusch *et al.*, 2009; Zasetsky *et al.*, 2009).

In the GS scenario, the PMC formation is thought to be controlled by temperature and water vapor, so a positive correlation between the ice particle radius and ice water content (*IWC*) is expected. However, this correlation is absent in

observations, for reasons that are still under debate (Megner, 2011; Megner, 2019; Wilms *et al.*, 2016; Wilms *et al.*, 2019).

95   What's more, satellite observations indicate a negative correlation between ice particle radius and albedo in the PMC regions affected by gravity waves (Gao *et al.*, 2018; Rusch *et al.*, 2017). Furthermore, the response of the ice particle radius in PMCs to the IMF B_y, as reported by Zhang et al. (2022), is also challenging to comprehend, given that the effects of the solar wind magnetic field are not incorporated into the GS scheme.

The PMC height is closely related to the fundamental processes of PMC formation, and is mainly determined by the

100   temperature structure in the upper mesosphere, with water vapor playing a minor role (Hervig *et al.*, 2009c; Russell III *et al.*, 2010). However, previous studies have focused on the effects of temperature and water vapor on the PMC formation, with little attention paid to the effect of PMC height. In this paper, we investigate the relationships for PMCs with altitude, temperature and latitude, based on which we propose the "charged-MSPs nucleation" scheme for PMC formation. The CMN scheme overcomes the limitations of the GS scheme, and provides new pathways to explain the response of PMCs to solar

105   activity and atmospheric dynamics.

2 Data and results

2.1 The PMC data

The PMC data applied in this work are observed by the Solar Occultation for Ice Experiment (SOFIE) and Cloud Imaging and Particle Size (CIPS) instruments on board the Aeronomy of Ice in the Mesosphere (AIM) satellite. Launched on 25 April

110   2007, the AIM satellite follows a sun-synchronous polar orbit and observes the PMC region approximately 15 times per day (Russell III *et al.*, 2009). The SOFIE platform performs occultation measurements to obtain vertical profiles of PMC properties, as well as the surrounding temperature and water vapor (Gordley *et al.*, 2009; Hervig *et al.*, 2009b). SOFIE covers regions at latitudes varying between 65° and 82° over time, and observes mainly around 70° latitude during the PMC season. The SOFIE provides polar mesospheric cloud data for 8 PMC seasons (from 2007 to 2014) in NH and 7 PMC

115   seasons (from 2007/2008 to 2013/2014) in SH, after which the SOFIE observes lower latitudes without PMCs. The CIPS platform consists of a panoramic UV nadir imager that observes the scattered radiance from PMCs, and images the PMCs in the 40°-85° latitude range with a horizontal spatial resolution of 5×5 km. The CIPS provides rectangular images of PMC properties in terms of ice particle radius, albedo, and *IWC* (Carstens *et al.*, 2013; Lumpe *et al.*, 2013). The CIPS data are available for 10 PMC seasons (from 2007 to 2016) in NH and 10 PMC seasons (from 2007/2008 to 2016/2017) in SH.

120   The SOFIE/AIM provides measurements for the altitude of the top (Z_{top}), maximum (Z_{max}) and bottom (Z_{bot}) of the ice layer in PMCs, as well as the altitude of the mesopause, as shown in Figure 1. The more frequent planetary waves in the NH cause stronger upward winds in the upper mesosphere, which adiabatically reduce the temperature and lead to an expansion of the saturation zone. Consequently, the altitude of the PMC bottom (Z_{bot}) observed by the SOFIE/AIM at about 70° latitude is approximately 1.7 km lower in the NH than in the SH, as shown in Fig. 1 and Table 1. The daily mean PMC height is

125   calculated by averaging the altitudes of the top and bottom of the PMC, $h = (Z_{top} + Z_{bot})/2$. The daily mean PMC thickness is

defined as the distance between the top and bottom of the PMC, $\Delta Z = Z_{top} - Z_{bot}$. The daily mean ice particle radius r and concentration N are calculated by averaging the ice particle radius and concentration inside the altitude range between the daily mean Z_{bot} and Z_{top}.

2.2 Effects of altitude

130　Figures 2 and 3 demonstrate a significant negative correlation between the anomaly of daily mean ice particle radius r and PMC height h in both the NH and SH. The data anomalies are obtained by removing the 35-day running mean, and the time span of -10 to 50 days from the solstice is applied to define the PMC season. Similarly, Figures 4 and 5 demonstrate significant positive correlations for the daily mean ice particle concentration N and the PMC height h. The mean sensitivity of r to h is about -3.2 nm/km in the NH and -2.6 nm/km in the SH, and the mean sensitivity of N to h is about 72.3 cm^{-3}/km

135　in the NH and 78.6 cm^{-3}/km in the SH. Figure 6 compares the mean correlation coefficients of the anomaly of r and N with h in all PMC seasons to that of the anomaly of r and N with ΔZ. In the GS scheme, both the lifetime of the falling ice particles in the supersaturated zone and the ice particle radius are expected to increase with increasing PMC thickness ΔZ. Meanwhile, the mean ice particle radius r and concentration N are not expected to vary with PMC height h in the GS scheme. In conclusion, the results presented in Fig. 6 demonstrate that the r and N are sensitive to h rather than ΔZ, which does not

140　support the GS scheme.

Figure 7 provides further insight into the zero-day lag time of the relationships for the ice particle radius r and concentration N with the PMC height h. In order to compare the results of CIPS and SOFIE, the variations in the ice particle radius and albedo observed by CIPS/AIM within the latitudes of 65° and 75° with respect to the PMC height h observed by SOFIE/AIM at about 70° are calculated and presented in Figure 8, with the 3-day smoothing applied. Fig. 8 shows that the

145　ice particle radius r observed by CIPS/AIM is also negatively correlated with h, in agreement with that of SOFIE. It is unexpected that the albedo observed by CIPS/AIM is also negatively correlated with h, which may be attributed to that some visible ice particles becoming subvisible as the mean ice particle radius r decreases with increasing PMC height h.

2.3 Effects of temperature and water vapor

To investigate the influence of the surrounding environment on the PMC, the mean environment temperature T and water

150　vapor H_2O between 78 km and 88 km are calculated. Figure 9 (a) displays that the mean environment temperature T mainly affects the PMC thickness ΔZ, but not affect the PMC height h and the ice particle radius r and concentration N. Figure 10 shows the correlation coefficients for Z_{bot} and Z_{top} with temperature and water vapor at different altitudes, providing a more detailed illustration of the relationships between h and ΔZ with the environment. Since the Z_{top} is negatively correlated with the temperature at higher altitudes (>84 km), and Z_{bot} is positively correlated with the temperature at lower altitudes (<82

155　km), as shown in Fig. 10 (a), the net effect is that the mean environment temperature T mainly influences ΔZ but not h.

Figure 11 shows that the *IWC* observed by SOFIE/AIM is not affected by the PMC height h, but is positively correlated with the mean environment T and the PMC thickness ΔZ.

The relationship between PMCs and water vapor is quite complex and ambiguous. The formation of ice particles in PMCs consumes water vapor, as illustrated by the negative correlation between *IWC* and H_2O in Fig. 11. The freeze-drying effect influences the distribution of wate vapor by transporting it to lower altitudes through sedimentation and sublimation (Hervig *et al.*, 2015; Lübken *et al.*, 2009). For higher PMC bottoms, the freeze-drying effect may be less pronounced due to the smaller ice particle radii and weaker sedimentation, leading to the slightly positive correlation between the Z_{bot} and the H_2O at higher altitudes in the SH shown in Fig. 10 (b). Variations in water vapor may in turn affect the PMC height, i.e., when more water vapor is transported to the PMC top by upward winds, the Z_{top} will increase accordingly, as shown by the slightly positive correlation between the mean environment water vapor H_2O and the PMC height h in Fig. 9 (b).

In summary, the mean environment temperature T exerts a significant influence on the PMC thickness ΔZ and *IWC*, whereas the mean environment temperature T and water vapor H_2O do not affect the ice particle radius r and concentration N. In the GS process, the formation of PMCs is generally thought to be controlled by the temperature and water vapor, so the results here are difficult to explain by the GS scheme.

2.4 Effects of latitude

Figure 12 shows the variations in *IWC*, ice particle radius, and ice particle column concentration obtained by CIPS/AIM with latitudes varying from 60° to 85°. The ice particle column concentration N_c is estimated by dividing the *IWC* by the ice particle mass, $N_c = IWC/M_{ice}$, where the ice particle mass is estimated from the ice particle radius r and the ice density ($\rho_{ice} \approx$ 0.92 g cm^{-3}), $M_{ice} = 4\pi r^3\rho_{ice}/3$. The PMC season in the CIPS/AIM data is defined as the time span from 0 to 40 days after the solstice, and the error bars represent the standard deviation of the means of the 10 PMC seasons.

It is well known that higher latitudes favor the formation of PMCs due to the stronger upwelling. As shown in Fig. 1 and Table 1, the thickness of PMCs is larger in the NH due to the stronger atmospheric disturbances there. Fig. 12 (a) and (b) demonstrate that the *IWC* and the ice particle radius r increase with latitude for both hemispheres, as expected. However, it is surprising that the ice particle column concentration N_c decreases with latitude in the SH, as shown in Fig. 12 (c). In the GS scenario, the lifetime and concentration of the falling ice particles should increase with the PMC thickness and thus with the latitude. In brief, the decrease of ice particle column concentration N_c with latitude in the SH poses another puzzle for the GS scheme.

3 Discussion

3.1 The "charged-MSPs nucleation" scheme for PMC formation

185 In order to elucidate the aforementioned results of PMC variations with altitude, temperature and latitude, we propose the "charged-MSPs nucleation" scheme for PMC formation, as illustrated in Figure 13. In the CMN scheme, the charged-MSPs act as ice nuclei by attracting water molecules through electric force, and ice nucleation occurs throughout the supersaturated region. The PMC is approximately in equilibrium with the surrounding environment, namely, the ice particles grow mainly in situ, with sedimentation playing a minor role. The ice particles continue to grow until the environment changes from

190 supersaturated to unsaturated due to the consumption of the local water vapor.

According to the thermodynamic equilibrium, the mass of ice (Q_{ice}) at a given altitude is roughly equal to the difference between the total water vapor content (Q_{tot}) and the saturated water vapor content (Q_{sat}). The ice particle size is determined by the competition for the limited water vapor ($\approx Q_{tot} - Q_{sat}$), so the ice particle radius r should be negatively correlated with the ice particle concentration N at any altitude, as shown in Figure 14. Previous observations and simulations attribute the

195 negative correlation between r and N at the Z_{max} to the competition for limited water vapor (Hervig *et al.*, 2009b; Hultgren and Gumbel, 2014; Wilms *et al.*, 2016). Fig. 14 extends this idea to each altitude, and supports the hypothesis that there is an excess of small charged-MSPs to act as ice nuclei for the entire PMC range. In the CMN scenario, a significant number of small ice particles in PMCs may be subvisible, providing an alternative explanation for the ice mass density estimated by thermodynamic equilibrium being higher than observed (Christensen *et al.*, 2016; Hervig *et al.*, 2009c).

200 The concentration of charged-MSPs increases rapidly with altitude, in accordance with the exponential increase in electron density produced by solar UV ionization. Therefore, the ice particle concentration N and radius r are mainly determined by the PMC height h, as shown in Fig. 6. For higher PMCs, more charged-MSPs are involved to act as ice nuclei and compete for the limited water vapor, resulting in smaller ice particles. Conversely, when PMCs occur at lower altitudes, fewer MSPs are charged by electrons, allowing ice particles to grow larger. This is consistent with the ground-based

205 observations that the lower PMCs are brighter (Gerding *et al.*, 2021; Ugolnikov and Maslov, 2019), possibly because the larger ice particles in the lower PMCs cause some subvisible ice particles to become visible.

The mean environment temperature T of the upper mesosphere between 78 km and 88 km mainly affects the PMC thickness ΔZ and IWC, but plays a minor role in the ice particle concentration N and radius r, as illustrated in Fig. 9 and Fig. 11. The temperature at higher altitudes (>84 km) exerts a negative influence on the Z_{top}, while the temperature at lower

210 altitudes (<82 km) exerts a positive influence on the Z_{bot}, as shown in Fig. 10 (a). Consequently, the net effect is that the mean environment temperature T primarily affects ΔZ, but not h. In other words, the PMC height h is influenced by the temperature structure rather than the mean temperature of the upper mesosphere.

It is worth noting that Hervig *et al.* (2009c) identified a negative correlation between the temperature T and ice particle concentration N at Z_{max}. However, we argue that this correlation does not imply causality. Rather, from the perspective of the

215 CMN scenario, it is due to the opposite response of T and N to PMC height h. On the one hand, temperature and water vapor decrease dramatically with altitude in the upper mesosphere, therefore, both the mean temperature T and water vapor measured within the PMC altitude range become smaller for higher PMCs, as evidenced by the negative correlations for T with h and H_2O with h shown in Figure 15. It should be noted that the mean temperature and water vapor at PMC altitude shown in Fig. 15 are obtained by averaging over the variable altitude range of the daily Z_{bot} and Z_{top}, rather than the fixed

220 range of 78 km and 88 km applied in Fig. 9. On the other hand, the mean ice particle concentration N is positively correlated with h, as shown in Fig. 6. In light of the aforementioned logic, it can be further argued that the positive correlation between r and H_2O at Z_{max} reported by Hervig *et al.* (2009a), as well as the positive correlation between r and T at Z_{max} reported by Hervig *et al.* (2009c), also do not represent causal relationships. Rather, they result from the responses of these variables to the PMC height h variations.

225 The unexpected decrease in the ice particle column concentration N_c with latitude, as shown in Fig. 12 (c), can be well explained in the CMN scenario. At higher latitudes, the stronger upward winds cause the Z_{max} to be lower, as illustrated in Fig. 1. This results in fewer charged-MSPs being encountered, which in turn leads to fewer ice particles being formed at the lower Z_{max}. The CIPS/AIM measures PMCs primarily through the radiation reflected near Z_{max}. As a result, the ice particle column concentration obtained by CIPS/AIM decreases with latitude in the SH. In the NH, perturbations from lower

230 atmospheres are stronger, and the Z_{max} observed by SOFIE/AIM near 70° is about 1.0 km lower, as shown in Fig. 1. Consequently, the reduction in Z_{max} from 60° to 85° should be less pronounced in the NH, resulting in a minimal change in N_c as depicted in Fig. 12 (c).

3.2 Comparison of the CMN scheme with the GS scheme

In the CMN scheme, the charged-MSPs act as ice nuclei, and the nucleation occurs throughout the PMC range. This is a

235 more reasonable scenario than the nucleation in the GS scheme, which occurs primarily at the top of the PMC. The concentration of MSPs varies exponentially with their radius, resulting in a greater number of small MSPs being available to attach electrons and act as ice nuclei in the CMN scenario, in contrast to the lack of large MSPs in the GS scenario due to meridional circulation transport.

The interpretation of the altitude distribution of ice particles in PMCs represents the primary distinction between the

240 CMN and GS schemes. In the CMN scenario, the observed increase in ice particle concentration N with altitude is attributed to the altitude distribution of charged-MSPs, and the opposite distribution of ice particle radius r is attributed to the competition for the limited water vapor, as illustrated in Fig. 13. In the GS scenario, the altitude distribution of N and r is primarily influenced by the growth and sedimentation of ice particles.

In contrast to the GS scenario, double-layer PMCs are permitted to form in the CMN scenario, provided that the

245 environment between the two layers is not conducive to PMC formation. In this case, ice particles in the upper and lower layers grow locally and independently. Furthermore, the mean ice particle radius in the lower layer is found to be larger than that in the upper layer (Gao *et al.*, 2017), which can be attributed to the fewer charged-MSPs in the lower PMCs. Stevens *et*

al. (2012) reported an inverse distribution of ice particle radius caused by rocket exhaust, which is unexplainable in the GS scenario. However, the CMN scenario offers a straightforward explanation for this phenomenon. The wate vapor injected by

250 space shuttles above 100 km diffuses downwards, providing more water vapor to form ice particles at the top of the PMC, leading to the formation of larger ice particles above the smaller ice particles.

In the CMN scenario, ice nucleation occurs at each altitude, and all ice particles grow in situ simultaneously, allowing the PMC to form rapidly. This is evidenced by the zero-day lag time shown in Fig. 7. In addition, the charges on MSPs and on small ice particles, the presence of which has been demonstrated by PMSEs, are expected to increase the nucleation and

255 growth rate, thereby contributing to the rapid changes in the PMC (Megner *et al.*, 2018; Rusch *et al.*, 2009; Zasetsky *et al.*, 2009). Nevertheless, the GS process requires a longer period for ice particles to grow and sediment over a distance of approximately 4 to 5 km from Z_{top} to Z_{bot} (Rusch *et al.*, 2017; Wilms *et al.*, 2016).

The lack of correlation between the ice particle radius r and the *IWC* is puzzling in the GS scheme (Megner, 2011; Megner, 2019; Wilms *et al.*, 2016; Wilms *et al.*, 2019), but straightforward in the CMN scheme: the ice particle radius r and

260 concentration N are sensitive to the PMC height h rather than to the mean environment temperature T, while the *IWC* and the PMC thickness ΔZ are controlled by the mean environment temperature T, as shown in Figs. 6, 9, and 11.

3.3 New pathways for solar activity and atmospheric dynamics affecting PMCs

The CMN scheme provides a new pathway for the solar activity to affect PMCs via the charging process of MSPs. Zhang *et al.* (2022) report a positive response of the ice particle radius r, *IWC* and albedo to the IMF B_y in the SH with a lag time of

265 about zero days, and an opposite but weak response in the NH. These results are difficult to understand in the GS scheme, however, they are readily explicable in the CMN scheme: the increase in IMF B_y induces an increase in the electric potential of the ionosphere in the SH, which reduces the concentration of electrons and the negatively charged-MSPs, ultimately leading to an increase in the ice particle radius. As the mean ice particle radius increases, some subvisible ice particles become visible, resulting in the positive response of the *IWC* and albedo of PMCs in the SH to the IMF B_y. In addition, the

270 zero-day time lag of the PMC response to the IMF B_y also confirms the rapid variation of the PMCs, as predicted by the CMN scheme.

Solar UV and IMF B_y are usually not well correlated. During the solar minimum, the 27-day solar UV cycle tends to weaken, while the variations in IMF B_y remain relative stable. Moreover, the charged-MSPs lag behind the IMF B_y by about zero days, while water vapor lags behind the solar UV by at least five days. To summarize, the influence of IMF B_y on PMCs

275 does not align with that of solar UV, thereby contributing to the obscure 27-day solar signal in PMCs. In addition, solar UV can also impact the charging process of MSPs by ionizing the upper mesosphere. The lag time of charged-MSPs in response to solar UV is shorter than that of water vapor, which may explain why the observed lag time of PMCs in response to the 27-day solar UV cycle is as short as 0-3 days (Dalin *et al.*, 2018; Robert *et al.*, 2010; Thurairajah *et al.*, 2017).

The CMN scheme also provides a new pathway for atmospheric dynamics to influence PMCs via the PMC height. In the

280 PMC regions affected by gravity waves, the ice particle radius r is significantly negatively correlated with the PMC

9

brightness (Gao *et al.*, 2018; Rusch *et al.*, 2017), which is unexplainable in the GS scenario. However, this relationship can be well explained in the CMN scenario. During the cold phase of GWs, more water vapor is transported upwards. On the one hand, the variations in temperature T and water vapor H_2O favor the formation of PMCs, resulting in an increase in ΔZ and albedo. On the other hand, the PMC height h increases as more water vapor is transported to the top of the PMC, as shown in

285 Fig. 9 (b), leading to the involvement of more charged-MSPs to act as ice nuclei, whose competition for the limited water vapor results in a decrease in the mean ice particle radius r. Similarly, during the warm phase of GWs, the PMC thickness ΔZ and albedo decrease due to the higher temperature T and reduced water vapor H_2O, while the mean ice particle radius r increases due to the lower PMC height h. In summary, as GWs pass through PMCs, both the PMC thickness ΔZ and PMC height h change in response, causing the PMC brightness and ice particle radius to vary in opposite ways.

290 Inter-hemispheric coupling is induced by the sudden stratospheric warming (SSW) events in the winter hemisphere, causing the downward circulation anomaly in the summer polar mesopause which adiabatically heats the air and reduces the water vapor. During the IHC, similar to the warm phase of GWs, the brightness of PMCs should decrease, while the radius of ice particles should increase. SSWs are frequent in the NH but rare in the SH, so that the IHC is expected to lead to larger fluctuations in PMC height and ice particle radius in the SH than in the NH, as supported by Figs. 2-5 and Table 1.

4 Conclusion

This study demonstrates that the charged-MSPs nucleation scheme can explain a number of puzzles in the growth-sedimentation scheme and is likely to be responsible for the formation of PMCs. In the CMN scenario, ice nucleation occurs at all altitudes within the saturation zone, with charged-MSPs acting as ice nuclei. The concentration of charged-MSPs increases with altitude in accordance with the electron density, and their competition for water vapor determines the radius

300 of ice particles. The PMC exists approximately in equilibrium with the environment, i.e., ice particles grow mainly in situ, with sedimentation playing a minor role. The thickness ΔZ, IWC, and albedo of the PMC are primarily influenced by the mean environment temperature T, while the ice particle concentration N and radius r are influenced by the PMC height h, which depends on the temperature structure in the upper mesosphere. For higher latitudes, the colder temperature results in the higher IWC and larger ice particle radius r, but the lower PMC height h results in fewer charged-MSPs and thus the

305 smaller ice particle column concentration N_c in the SH.

The CMN scenario provides a new pathway to understand the influence of atmospheric dynamics on PMCs. Specifically, the atmospheric disturbances can affect the PMC formation by modifying the PMC heights. This paper suggests that GWs and IHC can influence the PMC heights by altering the water vapor at the top of the PMC. Similarly, whether planetary waves and tides can also influence PMC formation through PMC heights should be investigated in future studies.

310 The CMN scenario also provides a new pathway to understand the response of PMCs to solar activity. In particular, the solar activity can affect the ice nucleation in PMCs by influencing the charging process of MSPs. On the one hand, the IMF B_y can induce vertical electric fields in the polar ionosphere, modulating the concentration of electrons and charged-MSPs in

the upper mesosphere, ultimately affecting the ice particle radius and the PMC brightness. On the other hand, the solar UV
can also modulate the concentration of charged-MSPs through ionization, but with a shorter time lag than the effects of
315   heating and photolysis. In order to extract solar signals in PMCs, future work should take into account both the effects of
IMF B_y and solar UV on the charged-MSPs.

In the future, a PMC model incorporating the CMN scheme should be developed to improve the microphysical
processes, as opposed to the GS scheme applied in the majority of current PMC models. To this end, a thorough
investigation of the distribution and charging process of MSPs is required, and the effects of atmospheric dynamics on PMC
320   height and solar activity on the charging process of MSPs should be taken into account.

Data Availability. The PMC data from SOFIE/AIM are available from the SOFIE website (http://sofie.gats-inc.com/sofie/index.php) and the PMC data from CIPS/AIM are available from the Laboratory for Atmospheric and Space Physics website (http://lasp.colorado.edu/aim/download/pmc/l2).

Author Contributions. Liang Zhang, Zhongfang Liu, and Brian Tinsley conceived the idea together. Liang Zhang analyzed
325   the data and drafted the manuscript. Zhongfang Liu and Brian Tinsley revised the paper.

Competing Interests. The authors declare that they have no conflict of interests.

References

330   Antonsen, T., Havnes, O., and Mann, I.: Estimates of the Size Distribution of Meteoric Smoke Particles From Rocket-Borne Impact Probes, J. Geophys. Res.-Atmos., 122, 12,353-312,365, https://doi.org/10.1002/2017JD027220, 2017.

Beig, G., Scheer, J., Mlynczak, M. G., and Keckhut, P.: Overview of the temperature response in the mesosphere and lower thermosphere to solar activity, Rev. Geophys., 46, https://doi.org/10.1029/2007RG000236, 2008.

Carstens, J. N., Bailey, S. M., Lumpe, J. D., and Randall, C. E.: Understanding uncertainties in the retrieval of polar
335   mesospheric clouds from the cloud imaging and particle size experiment in the presence of a bright Rayleigh background, J. Atmos. Sol.-Terr. Phy., 104, 197-212, https://doi.org/10.1016/j.jastp.2013.08.006, 2013.

Chandran, A., Rusch, D. W., Thomas, G. E., Palo, S. E., Baumgarten, G., Jensen, E. J., and Merkel, A. W.: Atmospheric gravity wave effects on polar mesospheric clouds: A comparison of numerical simulations from CARMA 2D with AIM observations, J. Geophys. Res.-Atmos., 117, https://doi.org/10.1029/2012JD017794, 2012.

340   Christensen, O. M., Benze, S., Eriksson, P., Gumbel, J., Megner, L., and Murtagh, D. P.: The relationship between polar mesospheric clouds and their background atmosphere as observed by Odin-SMR and Odin-OSIRIS, Atmos. Chem. Phys., 16, 12587-12600, https://doi.org/10.5194/acp-16-12587-2016, 2016.

Collins, R. L., Stevens, M. H., Azeem, I., Taylor, M. J., Larsen, M. F., Williams, B. P., Li, J., Alspach, J. H., Pautet, P.-D., Zhao, Y., and Zhu, X.: Cloud Formation From a Localized Water Release in the Upper Mesosphere: Indication of Rapid Cooling, J. Geophys. Res.-Space, 126, e2019JA027285, https://doi.org/10.1029/2019JA027285, 2021.

345

Dalin, P., Pertsev, N., Perminov, V., Dubietis, A., Zadorozhny, A., Zalcik, M., McEachran, I., McEwan, T., Černis, K., Grønne, J., Taustrup, T., Hansen, O., Andersen, H., Melnikov, D., Manevich, A., Romejko, V., and Lifatova, D.: Response of noctilucent cloud brightness to daily solar variations, J. Atmos. Sol.-Terr. Phy., 169, 83-90, https://doi.org/10.1016/j.jastp.2018.01.025, 2018.

350

Dawkins, E. C. M., Stober, G., Janches, D., Carrillo-Sánchez, J. D., Lieberman, R. S., Jacobi, C., Moffat-Griffin, T., Mitchell, N. J., Cobbett, N., Batista, P. P., Andrioli, V. F., Buriti, R. A., Murphy, D. J., Kero, J., Gulbrandsen, N., Tsutsumi, M., Kozlovsky, A., Kim, J. H., Lee, C., and Lester, M.: Solar Cycle and Long-Term Trends in the Observed Peak of the Meteor Altitude Distributions by Meteor Radars, Geophys. Res. Lett., 50, e2022GL101953, https://doi.org/10.1029/2022GL101953, 2023.

355

DeLand, M. T., and Thomas, G. E.: Evaluation of Space Traffic Effects in SBUV Polar Mesospheric Cloud Data, J. Geophys. Res.-Atmos., 124, 4203-4221, https://doi.org/10.1029/2018JD029756, 2019.

Duft, D., Nachbar, M., and Leisner, T.: Unravelling the microphysics of polar mesospheric cloud formation, Atmos. Chem. Phys., 19, 2871-2879, https://doi.org/10.5194/acp-19-2871-2019, 2019.

Fiedler, J., and Baumgarten, G.: Solar and lunar tides in noctilucent clouds as determined by ground-based lidar, Atmos.

360

Chem. Phys., 18, 16051-16061, https://doi.org/10.5194/acp-18-16051-2018, 2018.

France, J. A., Randall, C. E., Lieberman, R. S., Harvey, V. L., Eckermann, S. D., Siskind, D. E., Lumpe, J. D., Bailey, S. M., Carstens, J. N., and Russell III, J. M.: Local and Remote Planetary Wave Effects on Polar Mesospheric Clouds in the Northern Hemisphere in 2014, J. Geophys. Res.-Atmos., 123, 5149-5162, https://doi.org/10.1029/2017JD028224, 2018.

365

Gao, H., Li, L., Bu, L., Zhang, Q., Tang, Y., and Wang, Z.: Effect of Small-Scale Gravity Waves on Polar Mesospheric Clouds Observed From CIPS/AIM, J. Geophys. Res.-Space, 123, 4026-4045, https://doi.org/10.1029/2017JA024855, 2018.

Gao, H., Shepherd, G. G., Tang, Y., Bu, L., and Wang, Z.: Double-layer structure in polar mesospheric clouds observed from SOFIE/AIM, Ann. Geophys., 35, 295-309, https://doi.org/10.5194/angeo-35-295-2017, 2017.

370

Gerding, M., Baumgarten, G., Zecha, M., Lübken, F.-J., Baumgarten, K., and Latteck, R.: On the unusually bright and frequent noctilucent clouds in summer 2019 above Northern Germany, J. Atmos. Sol.-Terr. Phy., 217, 105577, https://doi.org/10.1016/j.jastp.2021.105577, 2021.

Gordley, L. L., Hervig, M. E., Fish, C., Russell III, J. M., Bailey, S., Cook, J., Hansen, S., Shumway, A., Paxton, G., Deaver, L., Marshall, T., Burton, J., Magill, B., Brown, C., Thompson, E., and Kemp, J.: The solar occultation for ice

375

experiment, J. Atmos. Sol.-Terr. Phy., 71, 300-315, https://doi.org/10.1016/j.jastp.2008.07.012, 2009.

Gumbel, J., and Karlsson, B.: Intra- and inter-hemispheric coupling effects on the polar summer mesosphere, Geophys. Res. Lett., 38, https://doi.org/10.1029/2011GL047968, 2011.

Gumbel, J., and Megner, L.: Charged meteoric smoke as ice nuclei in the mesosphere: Part 1—A review of basic concepts, J. Atmos. Sol.-Terr. Phy., 71, 1225-1235, https://doi.org/10.1016/j.jastp.2009.04.012, 2009.

380

Hervig, M. E., Berger, U., and Siskind, D. E.: Decadal variability in PMCs and implications for changing temperature and water vapor in the upper mesosphere, J. Geophys. Res.-Atmos., 121, 2383-2392, https://doi.org/10.1002/2015JD024439, 2016a.

Hervig, M. E., Deaver, L. E., Bardeen, C. G., Russell III, J. M., Bailey, S. M., and Gordley, L. L.: The content and composition of meteoric smoke in mesospheric ice particles from SOFIE observations, J. Atmos. Sol.-Terr. Phy.,

385

84-85, 1-6, https://doi.org/10.1016/j.jastp.2012.04.005, 2012.

Hervig, M. E., Gerding, M., Stevens, M. H., Stockwell, R., Bailey, S. M., Russell III, J. M., and Stober, G.: Mid-latitude mesospheric clouds and their environment from SOFIE observations, J. Atmos. Sol.-Terr. Phy., 149, 1-14, https://doi.org/10.1016/j.jastp.2016.09.004, 2016b.

Hervig, M. E., Gordley, L. L., Russell III, J. M., and Bailey, S. M.: SOFIE PMC observations during the northern summer of

390

2007, J. Atmos. Sol.-Terr. Phy., 71, 331-339, https://doi.org/10.1016/j.jastp.2008.08.010, 2009a.

Hervig, M. E., Gordley, L. L., Stevens, M. H., Russell III, J. M., Bailey, S. M., and Baumgarten, G.: Interpretation of SOFIE PMC measurements: Cloud identification and derivation of mass density, particle shape, and particle size, J. Atmos. Sol.-Terr. Phy., 71, 316-330, https://doi.org/10.1016/j.jastp.2008.07.009, 2009b.

Hervig, M. E., Malaspina, D., Sterken, V., Wilson Iii, L. B., Hunziker, S., and Bailey, S. M.: Decadal and Annual Variations in Meteoric Flux From Ulysses, Wind, and SOFIE Observations, J. Geophys. Res.-Space, 127, e2022JA030749, https://doi.org/10.1029/2022JA030749, 2022.

Hervig, M. E., Siskind, D. E., Bailey, S. M., Merkel, A. W., DeLand, M. T., and Russell III, J. M.: The Missing Solar Cycle Response of the Polar Summer Mesosphere, Geophys. Res. Lett., 46, 10132-10139, https://doi.org/10.1029/2019GL083485, 2019.

Hervig, M. E., Siskind, D. E., Bailey, S. M., and Russell III, J. M.: The influence of PMCs on water vapor and drivers behind PMC variability from SOFIE observations, J. Atmos. Sol.-Terr. Phy., 132, 124-134, https://doi.org/10.1016/j.jastp.2015.07.010, 2015.

Hervig, M. E., Stevens, M. H., Gordley, L. L., Deaver, L. E., Russell III, J. M., and Bailey, S. M.: Relationships between polar mesospheric clouds, temperature, and water vapor from Solar Occultation for Ice Experiment (SOFIE) observations, J. Geophys. Res.-Atmos., 114, https://doi.org/10.1029/2009JD012302, 2009c.

Hultgren, K., and Gumbel, J.: Tomographic and spectral views on the lifecycle of polar mesospheric clouds from Odin/OSIRIS, J. Geophys. Res.-Atmos., 119, 14,129-114,143, https://doi.org/10.1002/2014JD022435, 2014.

Kaifler, N., Baumgarten, G., Klekociuk, A. R., Alexander, S. P., Fiedler, J., and Lübken, F. J.: Small scale structures of NLC observed by lidar at 69°N/69°S and their possible relation to gravity waves, J. Atmos. Sol.-Terr. Phy., 104, 244-252, https://doi.org/10.1016/j.jastp.2013.01.004, 2013.

Karlsson, B., Randall, C. E., Benze, S., Mills, M., Harvey, V. L., Bailey, S. M., and Russell III, J. M.: Intra-seasonal variability of polar mesospheric clouds due to inter-hemispheric coupling, Geophys. Res. Lett., 36, https://doi.org/10.1029/2009GL040348, 2009.

Kirkwood, S., Dalin, P., and Réchou, A.: Noctilucent clouds observed from the UK and Denmark-Trends and variations over 43 years, Ann. Geophys., 26, 1243-1254, https://doi.org/10.5194/angeo-26-1243-2008, 2008.

Knappmiller, S., Rapp, M., Robertson, S., and Gumbel, J.: Charging of meteoric smoke and ice particles in the mesosphere including photoemission and photodetachment rates, J. Atmos. Sol.-Terr. Phy., 73, 2212-2220, https://doi.org/10.1016/j.jastp.2011.01.008, 2011.

Lam, M. M., and Tinsley, B. A.: Solar wind-atmospheric electricity-cloud microphysics connections to weather and climate, J. Atmos. Sol.-Terr. Phy., 149, 277-290, https://doi.org/10.1016/j.jastp.2015.10.019, 2016.

Li, Z.-y., Ma, J. X., Li, H., and Wu, J.: Multicomponent Diffusion of Dusty Plasma in PMSE Including the Growth of Dust Particles, J. Geophys. Res.-Space, 127, e2021JA030005, https://doi.org/10.1029/2021JA030005, 2022.

Liu, X., Yue, J., Xu, J., Yuan, W., Russell III, J. M., and Hervig, M. E.: Five-day waves in polar stratosphere and mesosphere temperature and mesospheric ice water measured by SOFIE/AIM, J. Geophys. Res.-Atmos., 120, 3872-3887, https://doi.org/10.1002/2015JD023119, 2015.

Liu, X., Yue, J., Xu, J., Yuan, W., Russell III, J. M., Hervig, M. E., and Nakamura, T.: Persistent longitudinal variations in 8 years of CIPS/AIM polar mesospheric clouds, J. Geophys. Res.-Atmos., 121, 8390-8409, https://doi.org/10.1002/2015JD024624, 2016.

Lübken, F.-J., Berger, U., and Baumgarten, G.: On the Anthropogenic Impact on Long-Term Evolution of Noctilucent Clouds, Geophys. Res. Lett., 45, 6681-6689, https://doi.org/10.1029/2018GL077719, 2018.

Lübken, F. J., Berger, U., and Baumgarten, G.: Stratospheric and solar cycle effects on long-term variability of mesospheric ice clouds, J. Geophys. Res.-Atmos., 114, https://doi.org/10.1029/2009JD012377, 2009.

Lumpe, J. D., Bailey, S. M., Carstens, J. N., Randall, C. E., Rusch, D. W., Thomas, G. E., Nielsen, K., Jeppesen, C., McClintock, W. E., Merkel, A. W., Riesberg, L., Templeman, B., Baumgarten, G., and Russell III, J. M.: Retrieval of polar mesospheric cloud properties from CIPS: Algorithm description, error analysis and cloud detection sensitivity, J. Atmos. Sol.-Terr. Phy., 104, 167-196, https://doi.org/10.1016/j.jastp.2013.06.007, 2013.

Megner, L.: Minimal impact of condensation nuclei characteristics on observable Mesospheric ice properties, J. Atmos. Sol.-Terr. Phy., 73, 2184-2191, https://doi.org/10.1016/j.jastp.2010.08.006, 2011.

440   Megner, L.: Comment on "Nucleation of Mesospheric Cloud Particles: Sensitivities and Limits" by L. Megner, J. Geophys. Res.-Space, 124, 3162-3166, https://doi.org/10.1029/2018JA025646, 2019.

Megner, L., and Gumbel, J.: Charged meteoric particles as ice nuclei in the mesosphere: Part 2: A feasibility study, J. Atmos. Sol.-Terr. Phy., 71, 1236-1244, https://doi.org/10.1016/j.jastp.2009.05.002, 2009.

Megner, L., Gumbel, J., Rapp, M., and Siskind, D. E.: Reduced meteoric smoke particle density at the summer pole – Implications for mesospheric ice particle nucleation, Adv. Space Res., 41, 41-49, 445   https://doi.org/10.1016/j.asr.2007.09.006, 2008a.

Megner, L., Siskind, D. E., Rapp, M., and Gumbel, J.: Global and temporal distribution of meteoric smoke: A two-dimensional simulation study, J. Geophys. Res.-Atmos., 113, https://doi.org/10.1029/2007JD009054, 2008b.

Megner, L., Stegman, J., Pautet, P.-D., and Taylor, M. J.: First Observed Temporal Development of a Noctilucent Cloud Ice Void, Geophys. Res. Lett., 45, 10,003-010,010, https://doi.org/10.1029/2018GL078501, 2018.

450   Miao, J., Gao, H., Kou, L., Zhang, Y., Li, Y., Chu, Z., Bu, L., and Wang, Z.: A Case Study of Midlatitude Noctilucent Clouds and Its Relationship to the Secondary-Generation Gravity Waves Over Tropopause Inversion Layer, J. Geophys. Res.-Atmos., 127, e2022JD036912, https://doi.org/10.1029/2022JD036912, 2022.

Plane, J. M. C.: Cosmic dust in the earth's atmosphere, Chem. Soc. Rev., 41, 6507-6518, https://doi.org/10.1039/C2CS35132C, 2012.

455   Plane, J. M. C., Gumbel, J., Kalogerakis, K. S., Marsh, D. R., and von Savigny, C.: Opinion: Recent developments and future directions in studying the mesosphere and lower thermosphere, Atmos. Chem. Phys., 23, 13255-13282, https://doi.org/10.5194/acp-23-13255-2023, 2023.

Plane, J. M. C., Saunders, R. W., Hedin, J., Stegman, J., Khaplanov, M., Gumbel, J., Lynch, K. A., Bracikowski, P. J., Gelinas, L. J., Friedrich, M., Blindheim, S., Gausa, M., and Williams, B. P.: A combined rocket-borne and ground-460   based study of the sodium layer and charged dust in the upper mesosphere, J. Atmos. Sol.-Terr. Phy., 118, 151-160, https://doi.org/10.1016/j.jastp.2013.11.008, 2014.

Rapp, M., and Lübken, F. J.: Polar mesosphere summer echoes (PMSE): Review of observations and current understanding, Atmos. Chem. Phys., 4, 2601-2633, https://doi.org/10.5194/acp-4-2601-2004, 2004.

Rapp, M., and Thomas, G. E.: Modeling the microphysics of mesospheric ice particles: Assessment of current capabilities 465   and basic sensitivities, J. Atmos. Sol.-Terr. Phy., 68, 715-744, https://doi.org/10.1016/j.jastp.2005.10.015, 2006.

Robert, C. E., von Savigny, C., Rahpoe, N., Bovensmann, H., Burrows, J. P., DeLand, M. T., and Schwartz, M. J.: First evidence of a 27 day solar signature in noctilucent cloud occurrence frequency, J. Geophys. Res.-Atmos., 115, https://doi.org/10.1029/2009JD012359, 2010.

Robertson, S., Dickson, S., Horányi, M., Sternovsky, Z., Friedrich, M., Janches, D., Megner, L., and Williams, B.: Detection 470   of meteoric smoke particles in the mesosphere by a rocket-borne mass spectrometer, J. Atmos. Sol.-Terr. Phy., 118, 161-179, https://doi.org/10.1016/j.jastp.2013.07.007, 2014.

Rong, P. P., Russell III, J. M., Hervig, M. E., and Bailey, S. M.: The roles of temperature and water vapor at different stages of the polar mesospheric cloud season, J. Geophys. Res.-Atmos., 117, https://doi.org/10.1029/2011JD016464, 2012.

Rusch, D., Thomas, G., Merkel, A., Olivero, J., Chandran, A., Lumpe, J., Carstans, J., Randall, C., Bailey, S., and Russell III, 475   J.: Large ice particles associated with small ice water content observed by AIM CIPS imagery of polar mesospheric clouds: Evidence for microphysical coupling with small-scale dynamics, J. Atmos. Sol.-Terr. Phy., 162, 97-105, https://doi.org/10.1016/j.jastp.2016.04.018, 2017.

Rusch, D. W., Thomas, G. E., McClintock, W., Merkel, A. W., Bailey, S. M., Russell III, J. M., Randall, C. E., Jeppesen, C., and Callan, M.: The cloud imaging and particle size experiment on the aeronomy of ice in the mesosphere mission: 480   Cloud morphology for the northern 2007 season, J. Atmos. Sol.-Terr. Phy., 71, 356-364, https://doi.org/10.1016/j.jastp.2008.11.005, 2009.

Russell III, J. M., Bailey, S. M., Gordley, L. L., Rusch, D. W., Horányi, M., Hervig, M. E., Thomas, G. E., Randall, C. E., Siskind, D. E., Stevens, M. H., Summers, M. E., Taylor, M. J., Englert, C. R., Espy, P. J., McClintock, W. E., and Merkel, A. W.: The Aeronomy of Ice in the Mesosphere (AIM) mission: Overview and early science results, J. 485   Atmos. Sol.-Terr. Phy., 71, 289-299, https://doi.org/10.1016/j.jastp.2008.08.011, 2009.

Russell III, J. M., Rong, P., Bailey, S. M., Hervig, M. E., and Petelina, S. V.: Relationship between the summer mesopause and polar mesospheric cloud heights, J. Geophys. Res.-Atmos., 115, https://doi.org/10.1029/2010JD013852, 2010.

Scales, W. A., and Mahmoudian, A.: Charged dust phenomena in the near-Earth space environment, Rep. Prog. Phys., 79, 106802, https://doi.org/10.1088/0034-4885/79/10/106802, 2016.

490 Schäfer, B., Baumgarten, G., and Fiedler, J.: Small-scale structures in noctilucent clouds observed by lidar, J. Atmos. Sol.-Terr. Phy., 208, 105384, https://doi.org/10.1016/j.jastp.2020.105384, 2020.

Shapiro, A. V., Rozanov, E., Shapiro, A. I., Wang, S., Egorova, T., Schmutz, W., and Peter, T.: Signature of the 27-day solar rotation cycle in mesospheric OH and H2O observed by the Aura Microwave Limb Sounder, Atmos. Chem. Phys., 12, 3181-3188, https://doi.org/10.5194/acp-12-3181-2012, 2012.

495 Siskind, D. E., Stevens, M. H., Hervig, M. E., and Randall, C. E.: Recent observations of high mass density polar mesospheric clouds: A link to space traffic?, Geophys. Res. Lett., 40, 2813-2817, https://doi.org/10.1002/grl.50540, 2013.

Stevens, M. H., Gumbel, J., Englert, C. R., Grossmann, K. U., Rapp, M., and Hartogh, P.: Polar mesospheric clouds formed from space shuttle exhaust, Geophys. Res. Lett., 30, https://doi.org/10.1029/2003GL017249, 2003.

500 Stevens, M. H., Lossow, S., Fiedler, J., Baumgarten, G., Lübken, F.-J., Hallgren, K., Hartogh, P., Randall, C. E., Lumpe, J., Bailey, S. M., Niciejewski, R., Meier, R. R., Plane, J. M. C., Kochenash, A. J., Murtagh, D. P., and Englert, C. R.: Bright polar mesospheric clouds formed by main engine exhaust from the space shuttle's final launch, J. Geophys. Res.-Atmos., 117, https://doi.org/10.1029/2012JD017638, 2012.

Tanaka, K. K., Mann, I., and Kimura, Y.: Formation of ice particles through nucleation in the mesosphere, Atmos. Chem. 505 Phys., 22, 5639-5650, https://doi.org/10.5194/acp-22-5639-2022, 2022.

Thurairajah, B., Thomas, G. E., von Savigny, C., Snow, M., Hervig, M. E., Bailey, S. M., and Randall, C. E.: Solar-induced 27-day variations of polar mesospheric clouds from the AIM SOFIE and CIPS experiments, J. Atmos. Sol.-Terr. Phy., 162, 122-135, https://doi.org/10.1016/j.jastp.2016.09.008, 2017.

Tinsley, B. A., and Heelis, R. A.: Correlations of atmospheric dynamics with solar activity evidence for a connection via the 510 solar wind, atmospheric electricity, and cloud microphysics, J. Geophys. Res.-Atmos., 98, 10375-10384, https://doi.org/10.1029/93JD00627, 1993.

Ugolnikov, O. S., and Maslov, I. A.: Polarization analysis and probable origin of bright noctilucent clouds with large particles in June 2018, Planet. Space Sci., 179, 104713, https://doi.org/10.1016/j.pss.2019.104713, 2019.

Vellalassery, A., Baumgarten, G., Grygalashvyly, M., and Lübken, F. J.: Greenhouse gas effects on the solar cycle response 515 of water vapour and noctilucent clouds, Ann. Geophys., 41, 289-300, https://doi.org/10.5194/angeo-41-289-2023, 2023.

Williams, E., and Mareev, E.: Recent progress on the global electrical circuit, Atmos. Res., 135-136, 208-227, https://doi.org/10.1016/j.atmosres.2013.05.015, 2014.

Wilms, H., Rapp, M., and Kirsch, A.: Nucleation of mesospheric cloud particles: Sensitivities and limits, J. Geophys. Res.-520 Space, 121, 2621-2644, https://doi.org/10.1002/2015JA021764, 2016.

Wilms, H., Rapp, M., and Kirsch, A.: Reply to Comment on "Nucleation of Mesospheric Cloud Particles: Sensitivities and Limits", J. Geophys. Res.-Space, 124, 3167-3172, https://doi.org/10.1029/2018JA025876, 2019.

Yu, F., Nadykto, A. B., Herb, J., Luo, G., Nazarenko, K. M., and Uvarova, L. A.: H2SO4–H2O–NH3 ternary ion-mediated nucleation (TIMN): kinetic-based model and comparison with CLOUD measurements, Atmos. Chem. Phys., 18, 525 17451-17474, https://doi.org/10.5194/acp-18-17451-2018, 2018.

Yu, F., and Turco, R. P.: Ultrafine aerosol formation via ion-mediated nucleation, Geophys. Res. Lett., 27, 883-886, https://doi.org/10.1029/1999GL011151, 2000.

Zasetsky, A. Y., Petelina, S. V., Remorov, R., Boone, C. D., Bernath, P. F., and Llewellyn, E. J.: Ice particle growth in the polar summer mesosphere: Formation time and equilibrium size, Geophys. Res. Lett., 36, 530 https://doi.org/10.1029/2009GL038727, 2009.

Zhang, L., Tinsley, B., and Zhou, L.: Responses of CIPS/AIM noctilucent clouds to the interplanetary magnetic field, Atmos. Chem. Phys., 22, 13355-13370, https://doi.org/10.5194/acp-22-13355-2022, 2022.

Table 1. The mean values of the PMC top (Z_{top}), PMC maximum (Z_{max}), PMC bottom (Z_{bot}), PMC height (h), PMC thickness (ΔZ), ice particle radius (r), ice particle concentration (N), and ice water content (IWC), as well as the standard deviations for the anomalous values after removing the 35-day running mean. The PMC data are observed by SOFIE/AIM at about 70° latitude.

	Z_{top}	Z_{max}	Z_{bot}	h	ΔZ	r	N	IWC
SH	86.6 km	84.5 km	82.5 km	84.5 km	4.2 km	25.2 nm	296 cm^{-3}	28.5 μg/m^2
NH	86.5 km	83.5 km	80.8 km	83.7 km	5.7 km	27.0 nm	317 cm^{-3}	57.5 μg/m^2
	δZ_{top}	δZ_{max}	δZ_{bot}	δh	$\delta \Delta Z$	δr	δN	δIWC
SH	0.89 km	0.81 km	1.0 km	0.84 km	0.95 km	5.6 nm	242 cm^{-3}	12.8 μg/m^2
NH	0.65 km	0.54 km	0.82 km	0.59 km	0.89 km	3.6 nm	182 cm^{-3}	17.8 μg/m^2
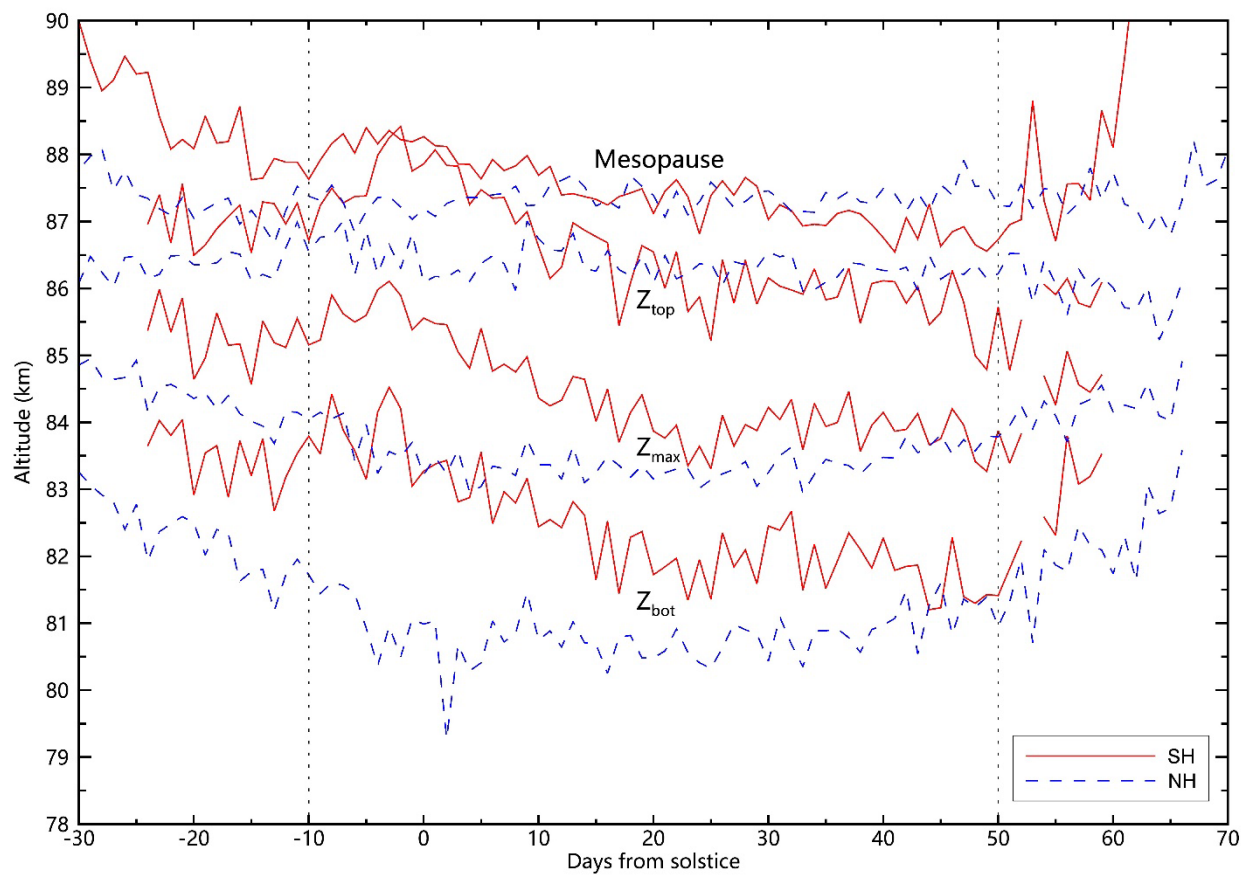
Figure 1. The altitudes of the top (Z_{top}), maximum (Z_{max}) and bottom (Z_{bot}) of the ice layer in PMCs, as well as the altitude of the mesopause. The PMC data are observed by the SOFIE/AIM at about 70° latitude.
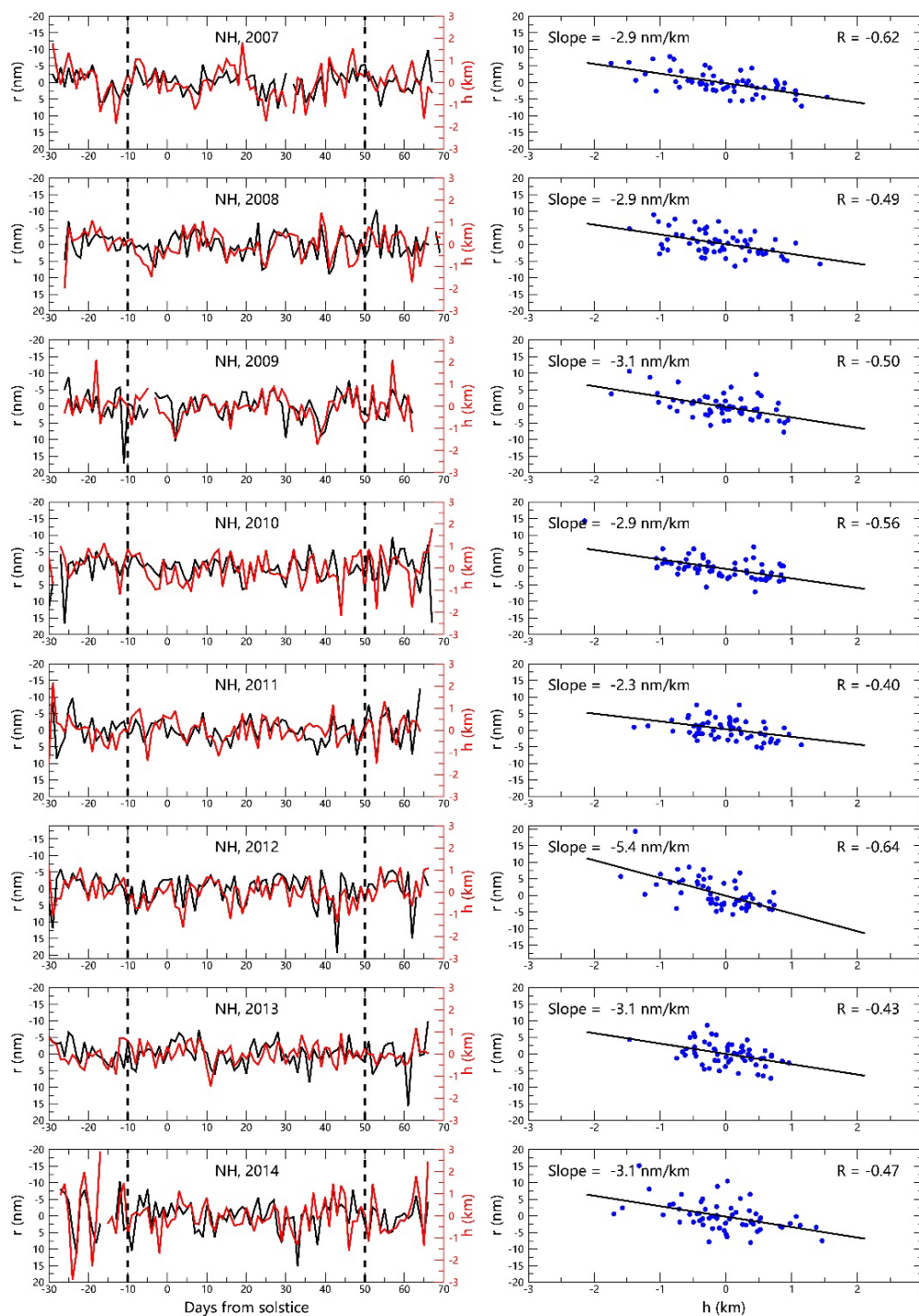
Figure 2. Left panels show the anomaly of the mean ice particle radius (*r*) and PMC height (*h*) in the NH from 2007 through 2014. Right panels show the corresponding correlation coefficients for the time span of -10 to 50 days from the solstice. The PMC data are observed by the SOFIE/AIM at about 70° latitude, and the 35-day running mean are removed.
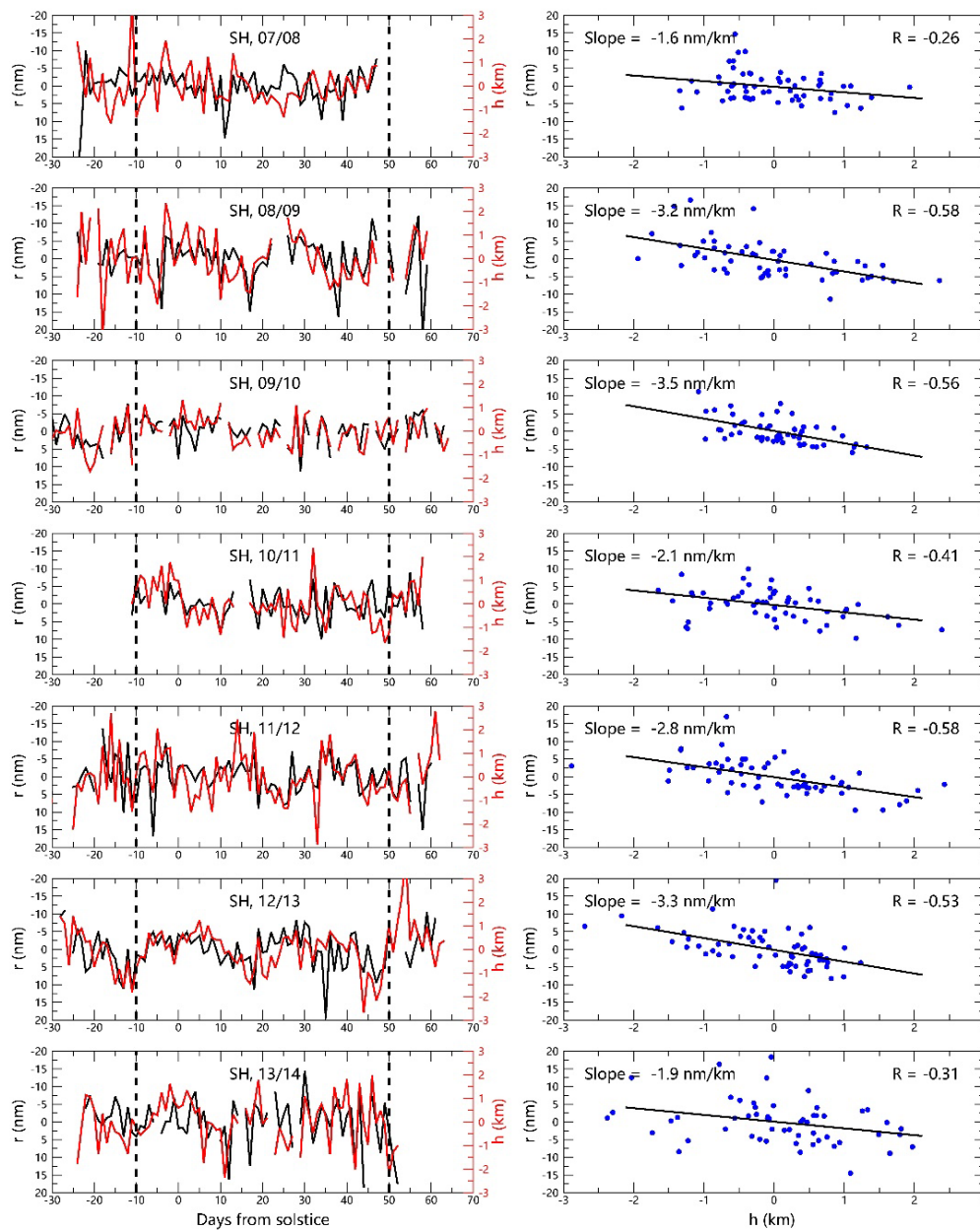
Figure 3. Similar to Fig. 2, but for that of the SH.

550
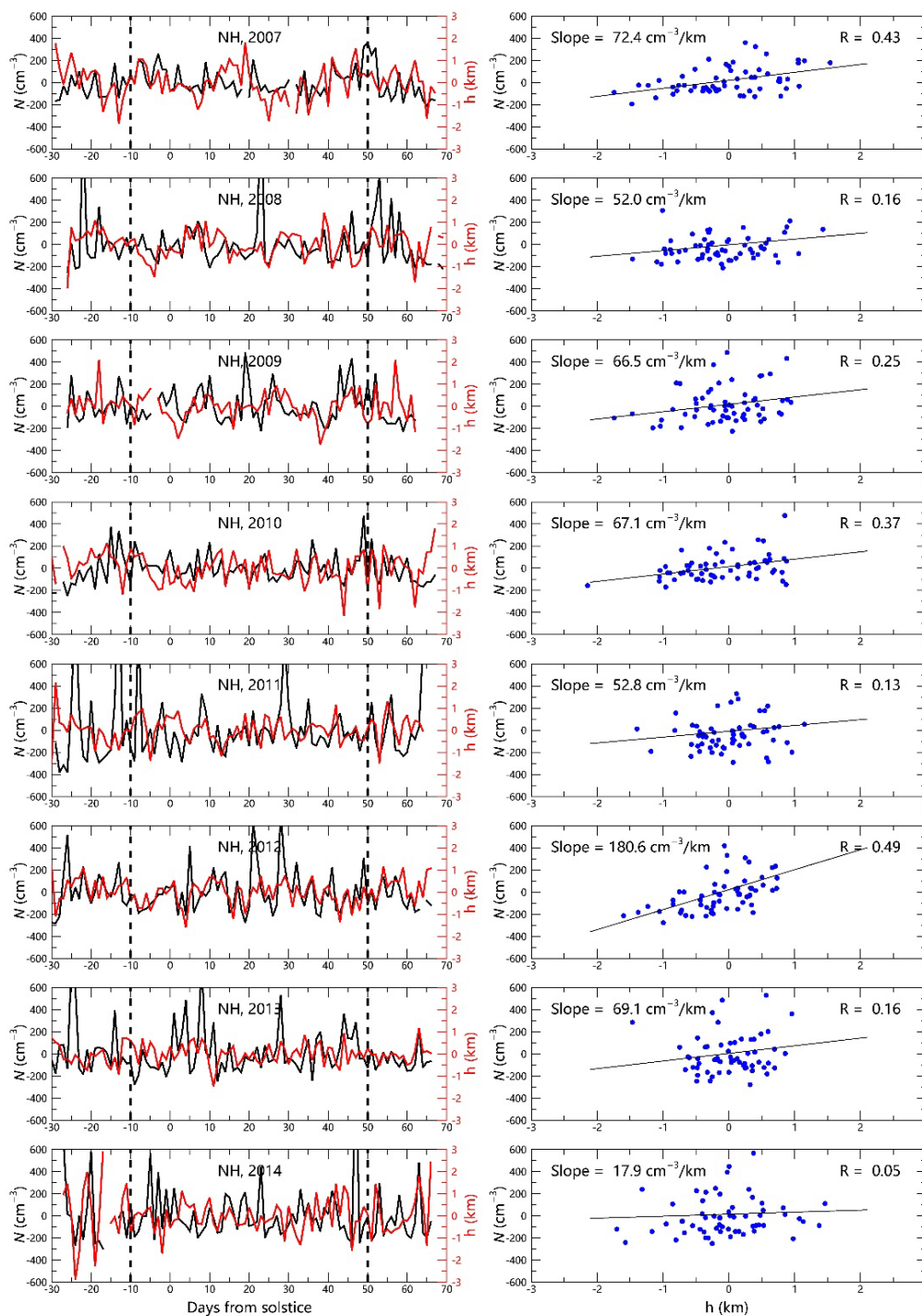
Figure 4. Similar to Fig. 2, but for that of the mean ice particle concentration (*N*).
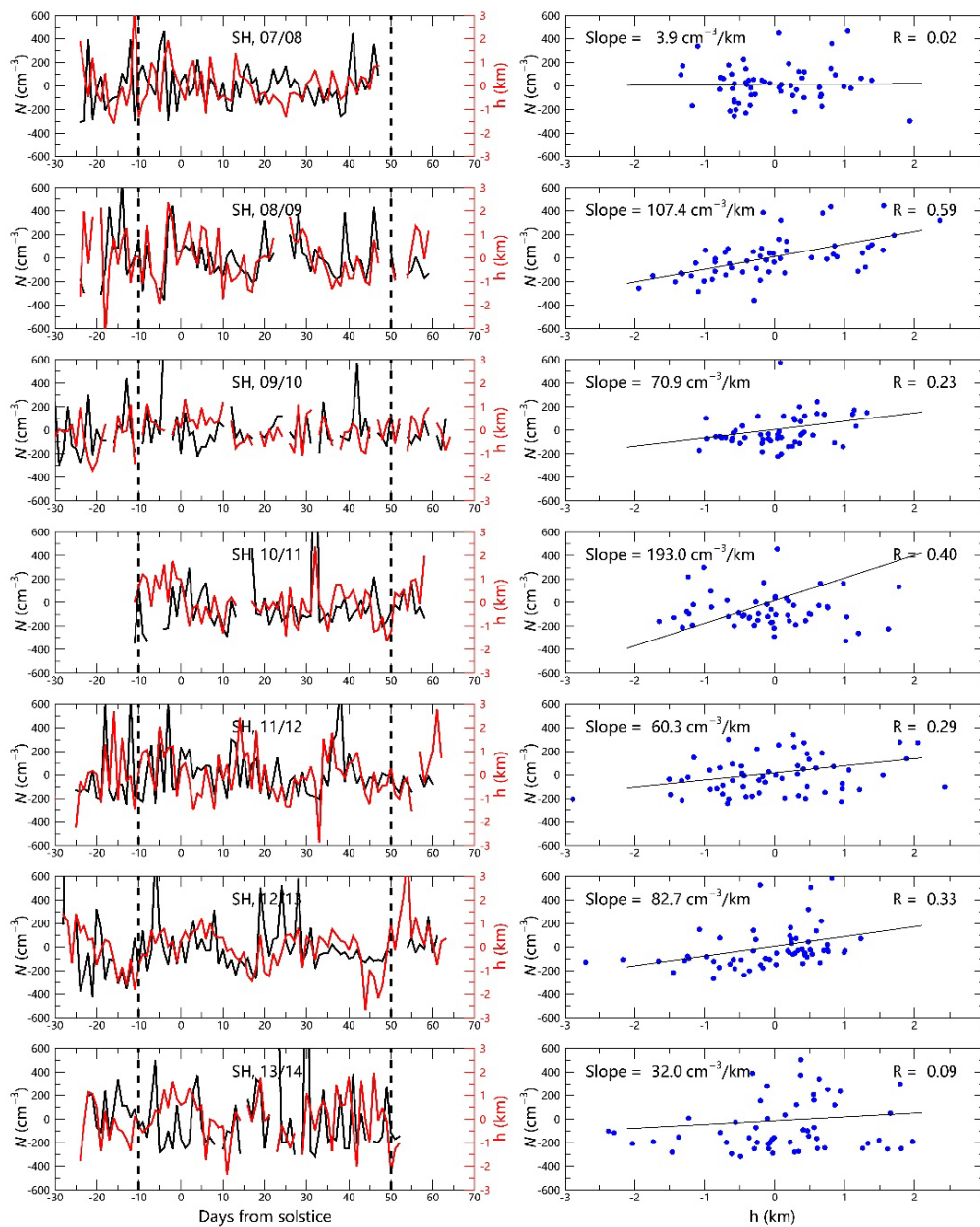
Figure 5. Similar to Fig. 4, but for that of the SH.
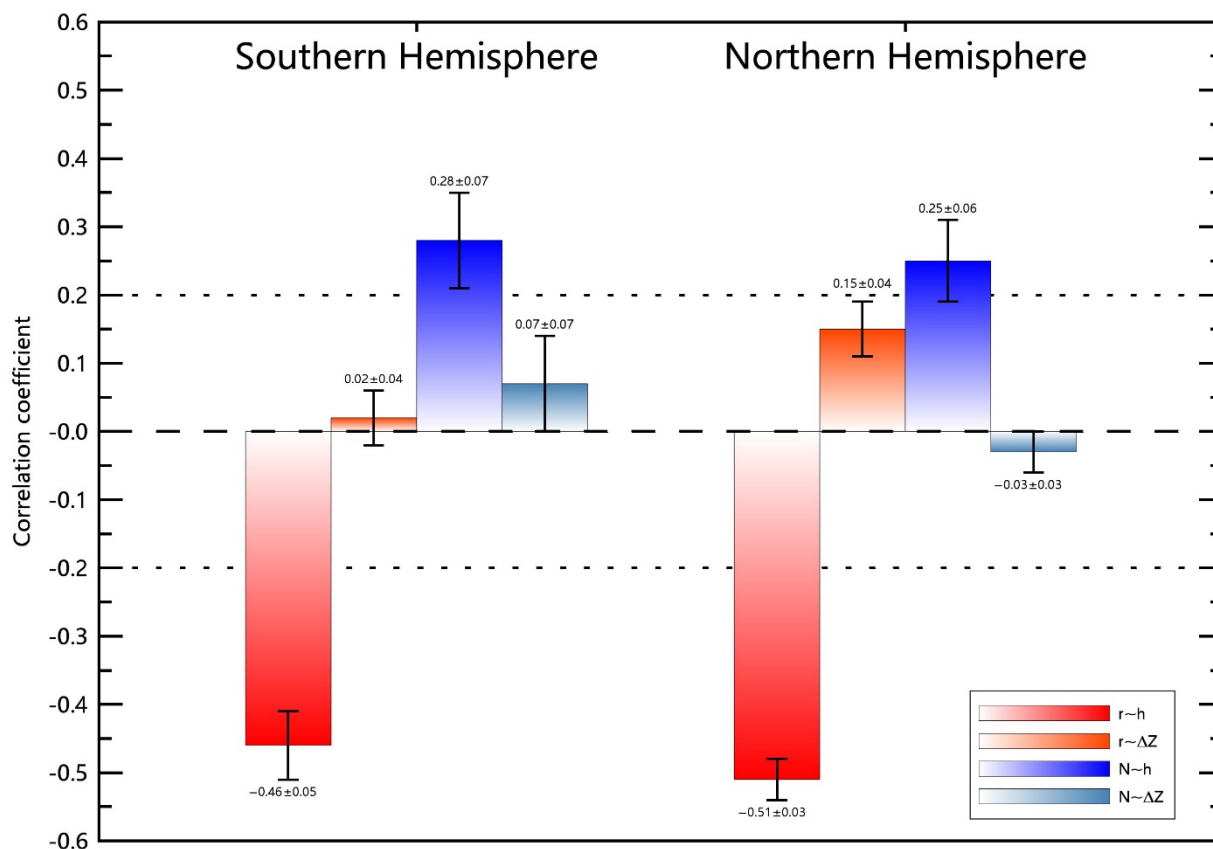
Figure 6. The correlation coefficients and the sensitivity for the mean ice particle radius (r) and concentration (N) with the PMC height (h) and thickness (ΔZ) for both hemispheres. The anomaly of the PMC data is obtained by removing the 35-day running mean. The PMC data are observed by the SOFIE/AIM at about 70° latitude.
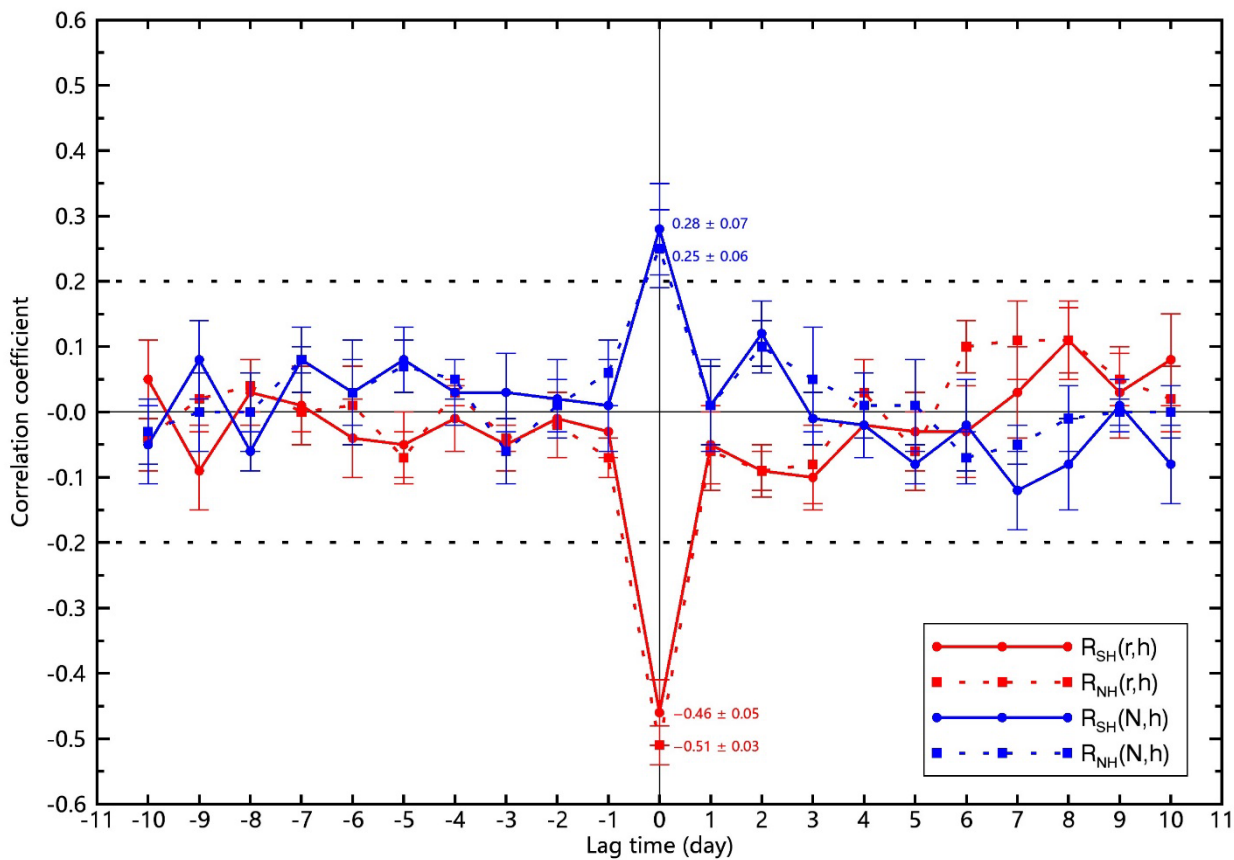
Figure 7. The correlation coefficients for the mean ice particle radius (*r*) and concentration (*N*) with the PMC height (*h*) for both hemispheres, with lag time varying from -10 to 10 days. The error bars illustrate the standard deviation of the means.
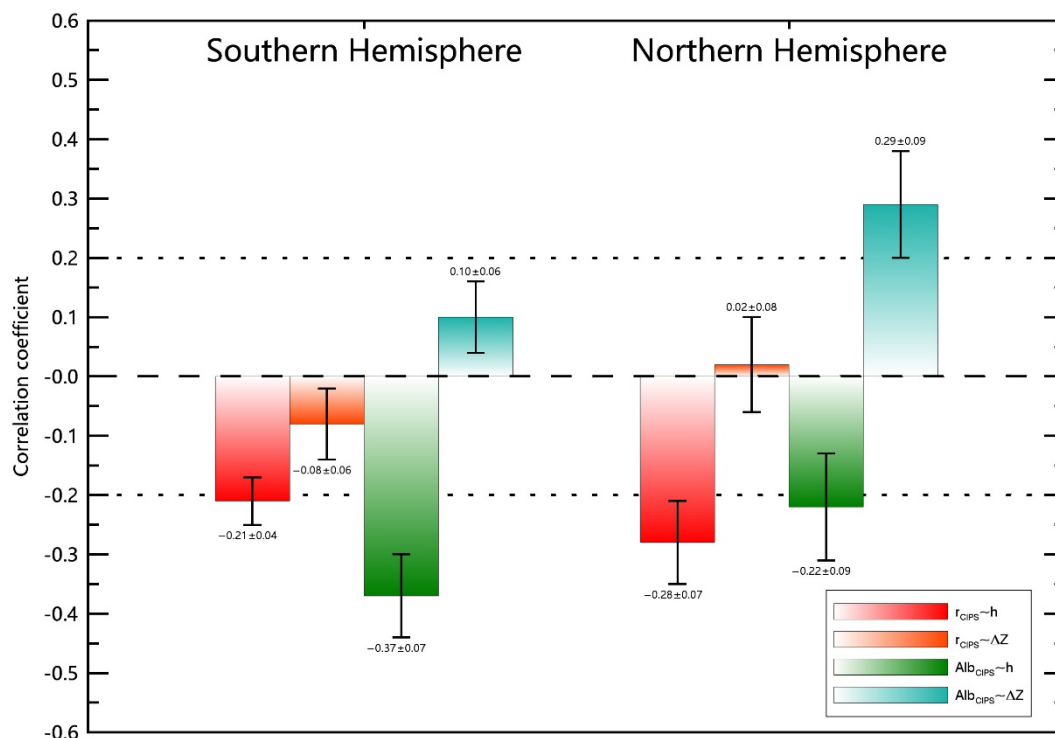
Figure 8. The correlation coefficients for the mean ice particle radius (r_{CIPS}) and albedo (Alb_{CIPS}) observed by CIPS/AIM at latitudes ranging from 65° to 75°, with the PMC height (h) and thickness (ΔZ) observed by the SOFIE/AIM at about 70° latitude for both hemispheres.
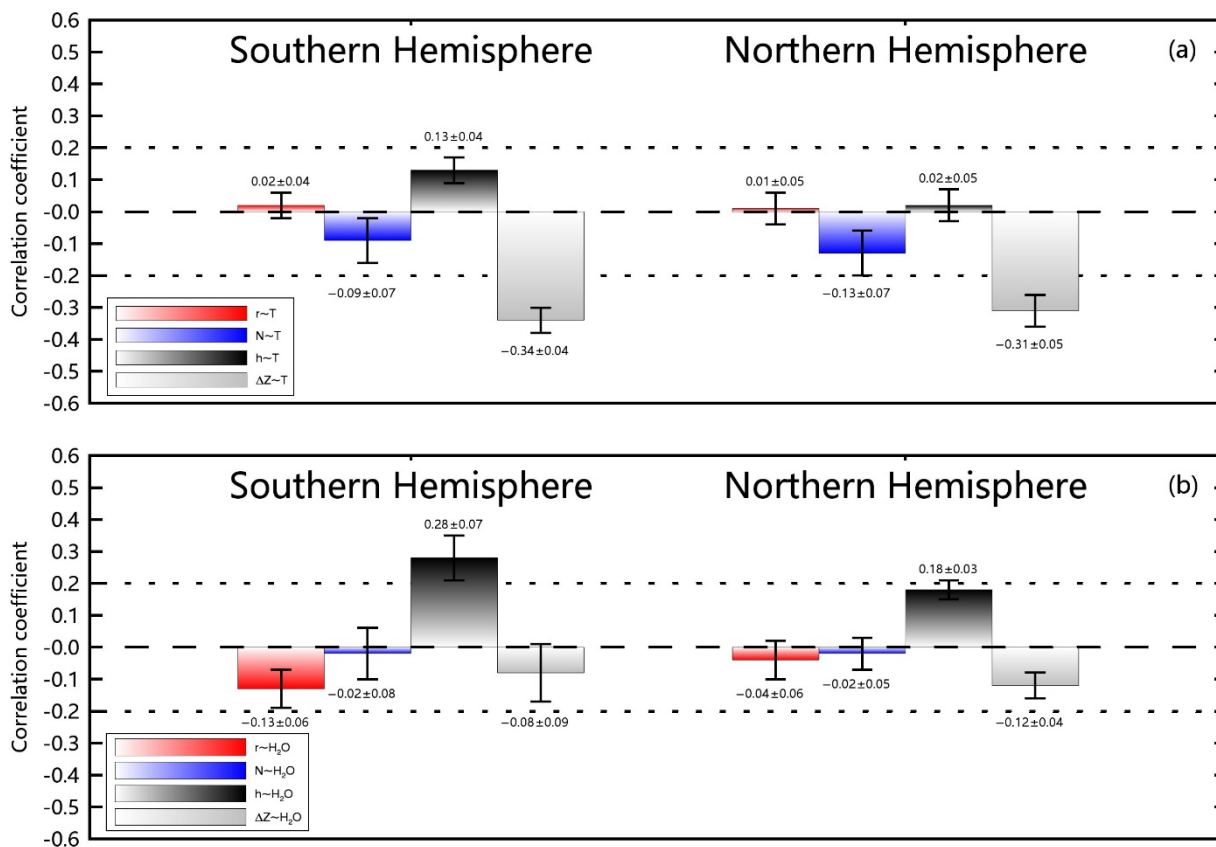
Figure 9. The correlation coefficients for the mean ice particle radius (r), concentration (N), PMC height (h), thickness (ΔZ) with the mean temperature (T) and water vapor (H_2O) between 78 km and 88 km. The PMC data are observed by the SOFIE/AIM at about 70° latitude.
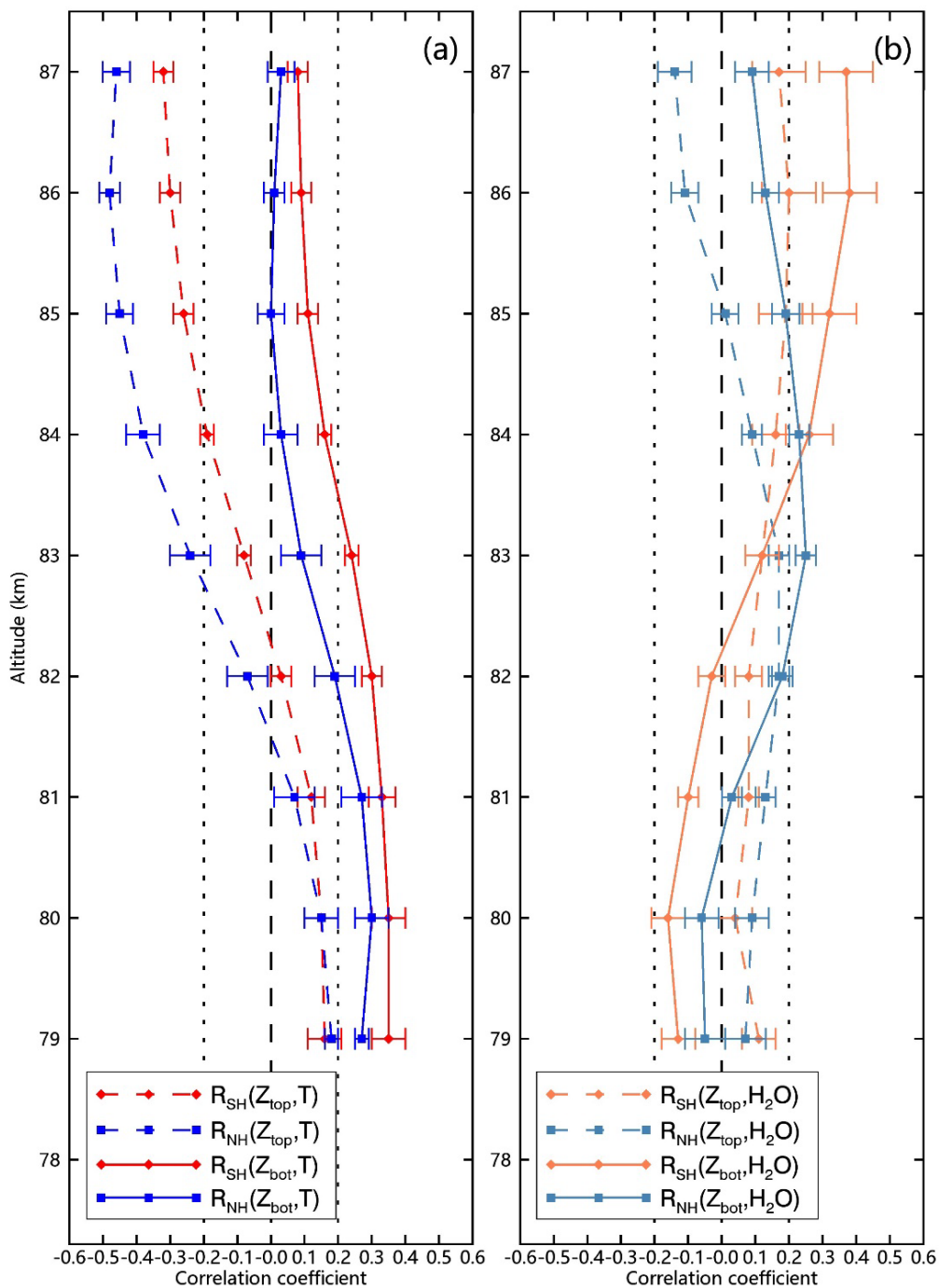
Figure 10. The correlation coefficients for the altitudes of PMC top (Z_{top}) and bottom (Z_{bot}) with the temperature and water vapor at varying altitudes.
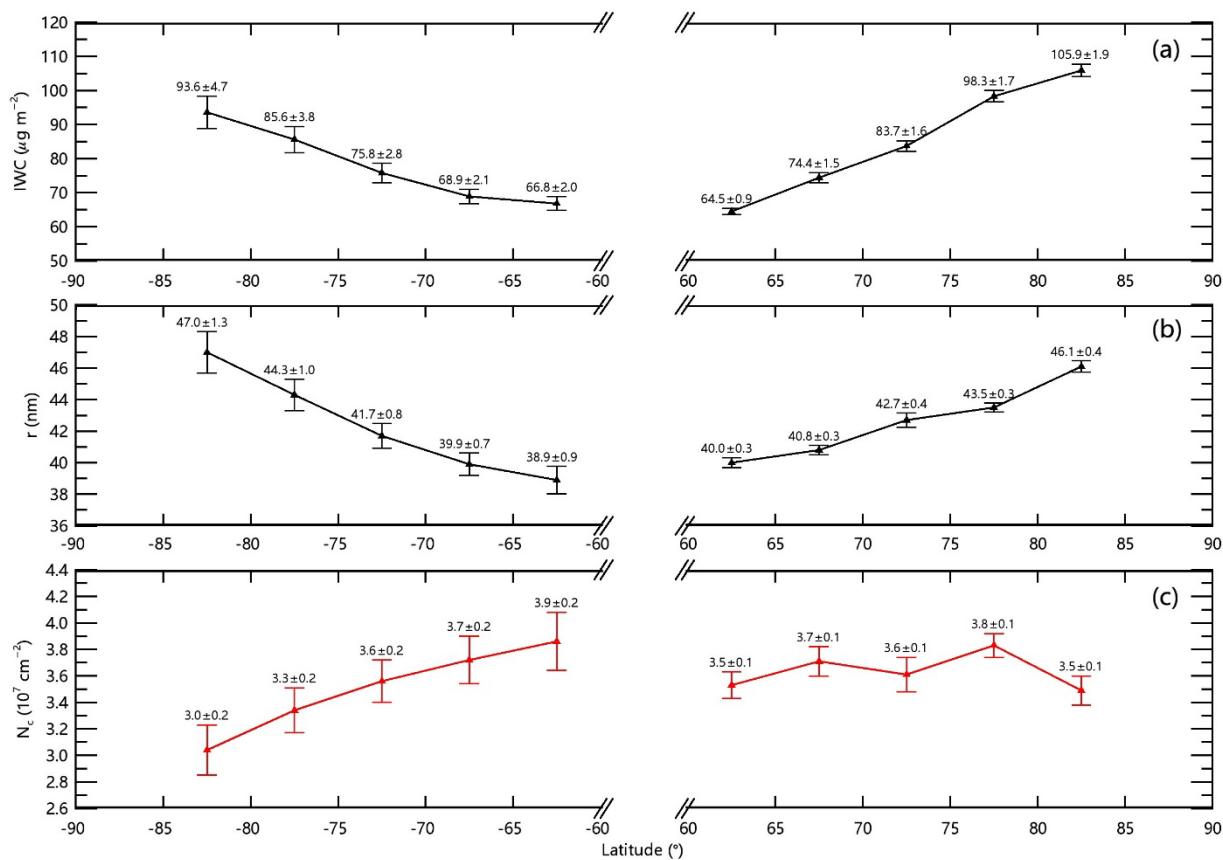
580
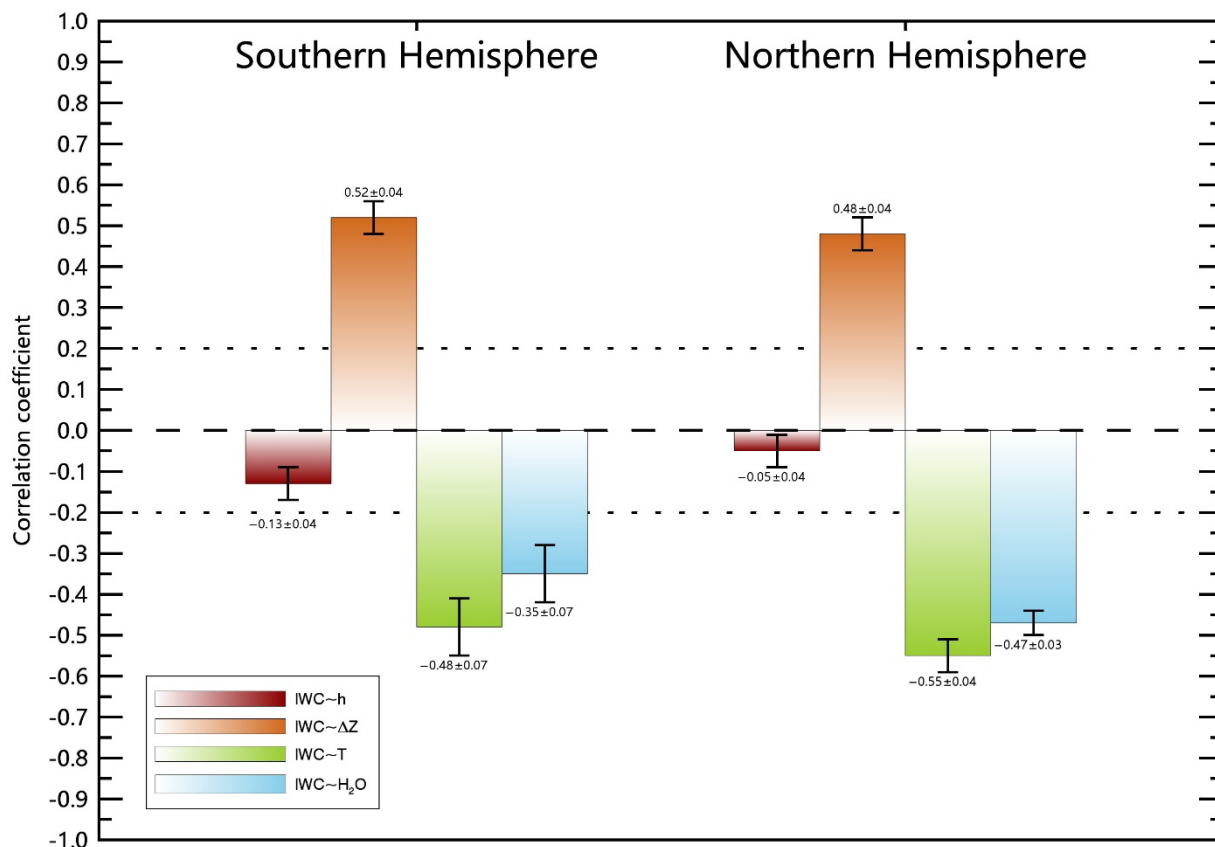
Figure 11. The correlation coefficients for the ice water content (*IWC*) with the PMC height (*h*), thickness (*ΔZ*), the mean temperature (*T*) and water vapor (*H₂O*) between 78 km and 88 km. The PMC data are observed by the SOFIE/AIM at about 70° latitude.
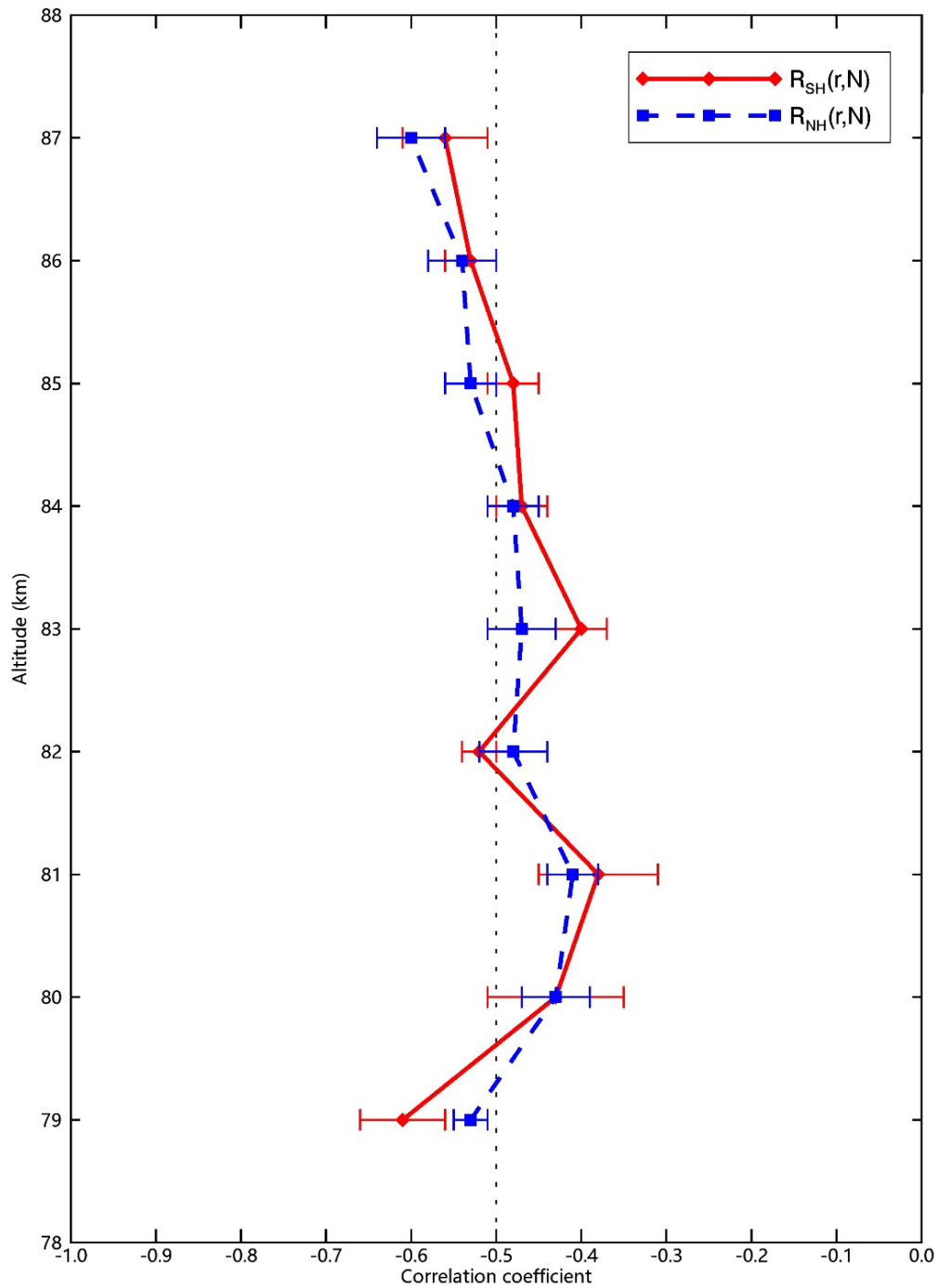
585

Figure 12. The variations of ice water content (*IWC*), ice particle radius (*r*), and ice particle column concentration (N_c) with latitude for both hemispheres. The PMC data are observed by the CIPS/AIM.
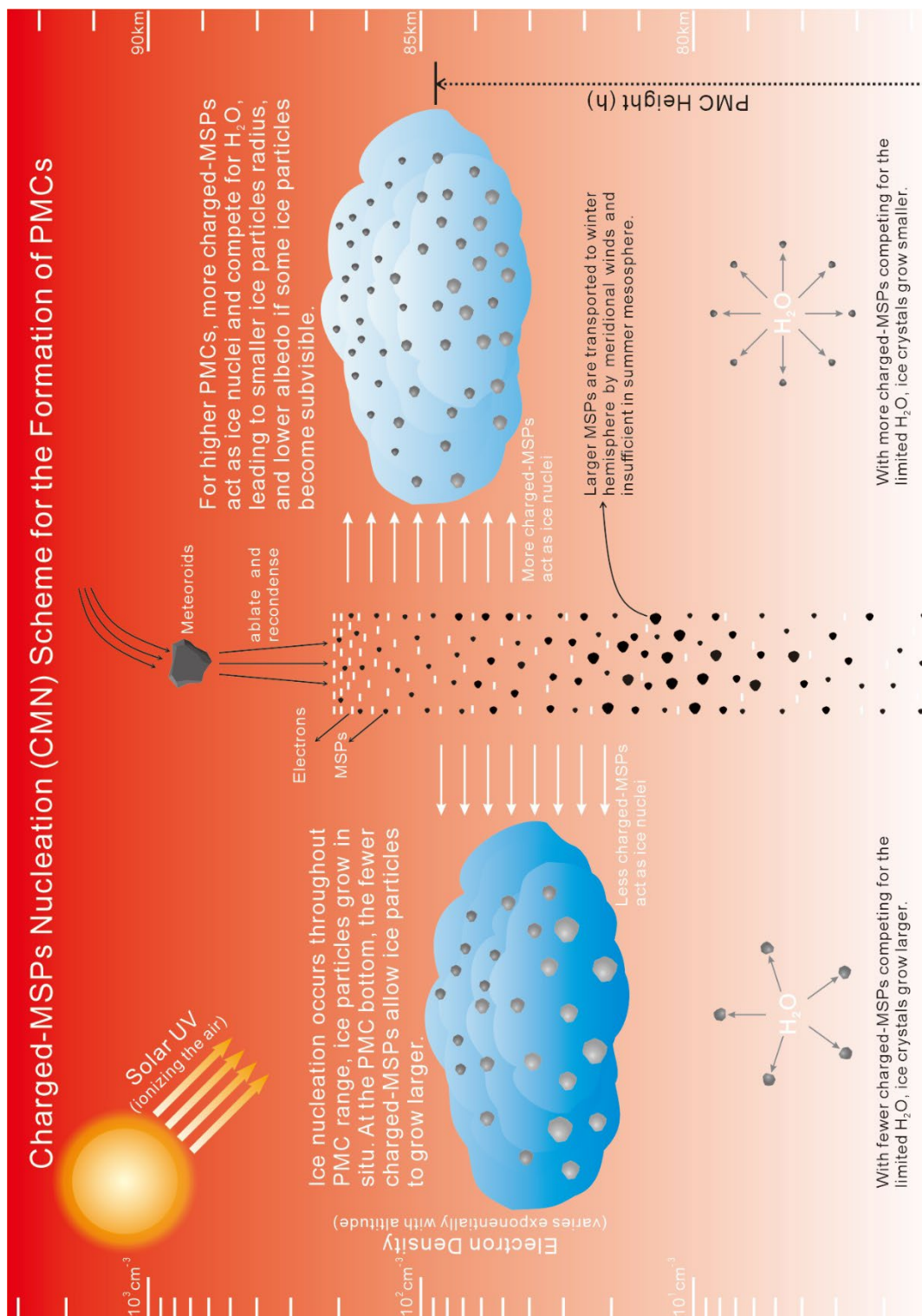
Figure 13. A schematic of the charged-MSPs nucleation (CMN) scheme for the PMC formation.

Figure 14. The correlation coefficients between the mean ice particle radius (*r*) and concentration (*N*) for altitudes between 79 km and 87 km for both hemispheres. The PMC data are observed by the SOFIE/AIM at about 70° latitude.
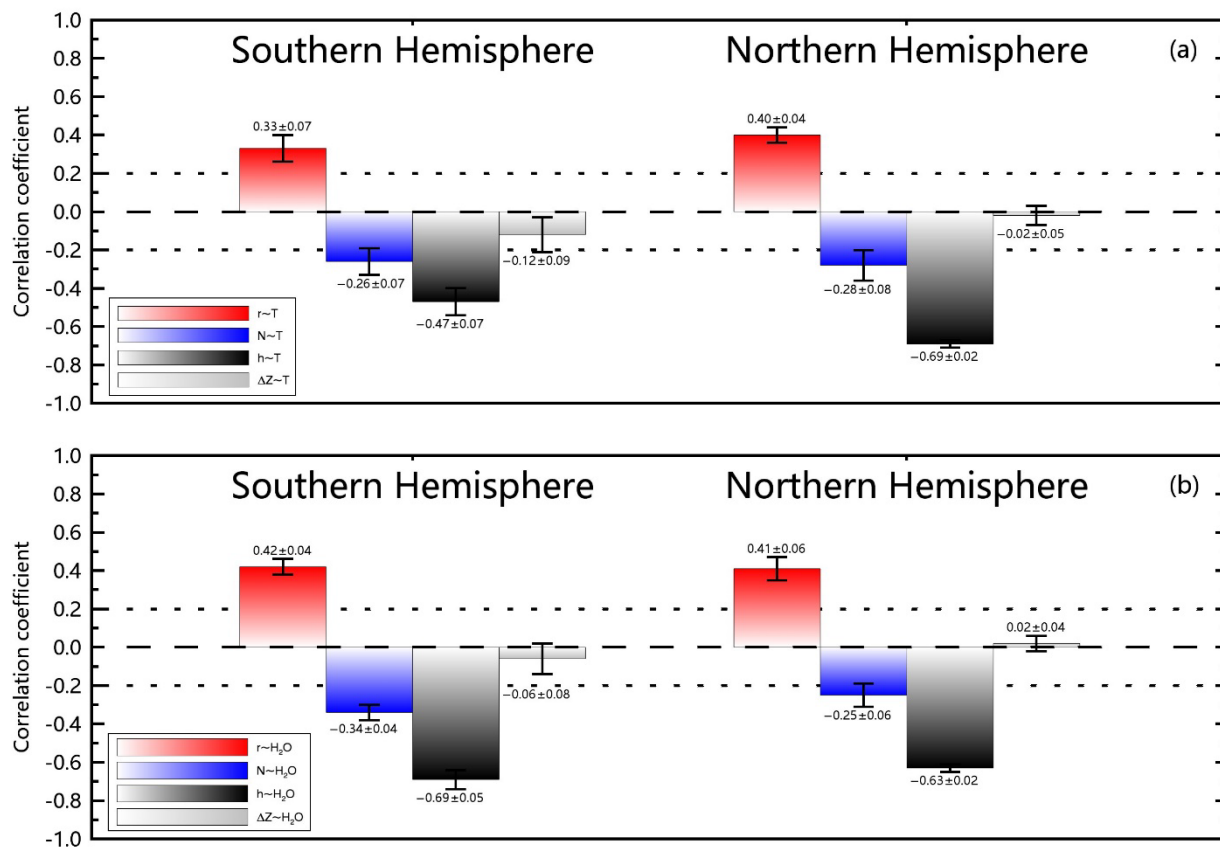
Figure 15. Similar to Fig. 9, but the daily mean temperature (T) and water vapor (H_2O) are averaged between the daily mean Z_{bot} and Z_{top}, rather than between 78 km and 88 km. The PMC data are observed by the SOFIE/AIM at about 70° latitude.